https://ntrs.nasa.gov/search.jsp?R=19660009167 2018-07-21T18:03:45+00:00Z

TECH LIBRARY KAFB, NM
0099535

NASA CONTRACTOR REPORT

NASA CR-395

NASA CR-539

INVESTIGATION OF THE TURBULENT SHEAR FLOW OF DILUTE AQUEOUS CMC SOLUTIONS

by W. D. Ernst

RECEIVED
18 MAR 1966
Technical Library
AF Weapons
Laboratory

Prepared under Contract No. NASw-729 *by*
LING-TEMCO-VOUGHT RESEARCH CENTER
Dallas, Texas
for

NATIONAL AERONAUTICS AND SPACE ADMINISTRATION • WASHINGTON, D. C. • MARCH 1966

TECH LIBRARY KAFB, NM

0099535

NASA CR-395

INVESTIGATION OF THE TURBULENT SHEAR FLOW OF DILUTE AQUEOUS CMC SOLUTIONS

By W. D. Ernst

Distribution of this report is provided in the interest of information exchange. Responsibility for the contents resides in the author or organization that prepared it.

Prepared under Contract No. NASw-729 by
LING-TEMCO-VOUGHT RESEARCH CENTER
Dallas, Texas

for

NATIONAL AERONAUTICS AND SPACE ADMINISTRATION

For sale by the Clearinghouse for Federal Scientific and Technical Information
Springfield, Virginia 22151 – Price $3.00

ABSTRACT

Experimental measurements of the fully developed turbulent flow field in straight circular tubes of dilute CMC solutions are described. Having a non-Newtonian power law exponent of 0.93 to 0.95, the viscosity of the solutions used was nearly Newtonian. Both pressure drop and velocity profile measurements were made over a wide range of Reynolds numbers. The velocity data was taken in both the linear sublayer and the turbulent core, and is presented in terms of the universal velocity parameters modified by use of a viscosity defined at the tube wall. A check of the existing empirical correlations based on a power law viscosity shows none predicting the observed velocity profiles.

CONTENTS

	Page
INTRODUCTION	1
FLUID CHARACTERISTICS	3
Additive Selection	3
Mixing and Handling	6
Properties	7
EXPERIMENTAL APPARATUS AND PROCEDURES	9
Facility	9
Instrumentation	10
Test Procedures	12
RESULTS AND DISCUSSION	12
Velocity Measurements	16
Friction Factor Measurements	21
CONCLUSIONS	23
ACKNOWLEDGEMENT	24
NOTATION	24
LITERATURE CITED	25
APPENDIX I	27
FIGURES	33

INTRODUCTION

Fluid dynamicists have been confronted with many new problems, both theoretical and experimental, with the advent of non-Newtonian rheology. The area chosen for the subject experimental study is the turbulent constrained flow of an elastico-viscous liquid. This flow field is of special interest since elastico-viscous liquids flow with an energy loss due to friction smaller than that experienced by Newtonian liquids at comparable Reynolds numbers. In addition, the fluid dynamicist is interested in this problem because it may shed some light on the mechanism of turbulence for a Newtonian liquid.

While most fluids are completely described by the linear relationship between the shear stress and shear rate, called Newton's law of viscosity, non-Newtonian fluids have either an additional property or a nonlinear functional relationship between the shear stress and shear rate, or both (1,2). There has been a significant amount of work published on purely viscous non-Newtonian fluids which agrees with the semi-theoretical expressions derived (3,4). These fluids appear to have a friction factor versus Reynolds number dependence that is independent of pipe diameter. The nonlinear functional relation most often used to characterize the properties of a purely viscous liquid is the power law relation (5),

$$\tau = a \left(\frac{du}{dy}\right)^n \qquad (1)$$

This relation, however, does not describe any of the unequal normal stresses appearing in many fluids.

An elastico-viscous fluid has a non-Newtonian rheology that gives it one of the properties of a solid, elasticity, and may or may not have a nonlinear shear stress versus shear rate relationship (6,7,8). Elasticity gives the fluid the ability to store energy reversibly and induces normal stresses. A complete description of a fluid's properties, a constitutive equation, when expressed in a tensor form must obey certain laws of invariance, making the material constants or properties of the constitutive equation difficult to evaluate experimentally (9, 10, 11). As yet, there is no means of measuring the constants necessary for describing the properties as predicted from the more complete, and therefore, more complicated sets of constitutive equations for elastico-viscous fluids. The only instance of success involves the correlation of the normal stresses in laminar flow with the shear reduction in turbulent flow (12). All existing data for fluids which are classified as being elastico-viscous indicate that, unlike the purely viscous fluid, the friction factor versus Reynolds number correlation is dependent on tube diameter (4,13).

Specifically, this report describes an experimental study of dilute (0.05% by weight) concentrations of CMC 7HSP flowing in tubes of two different diameters (0.650" ID and 1.427" ID) with a flow rate between 1.5 gal./min. and 275 gal./min. Measurements of

pressure drop, viscosity, and bulk velocity allowed a calculation of the friction factor for Reynolds numbers, based on a power law viscosity, from 6.0×10^3 to 4.6×10^5. Velocity profiles were determined at six Reynolds numbers in the large pipe and seven in the small pipe (using a probe .005" thick which allowed measurements close to the wall) in order to test the conventional relationship between Φ and η, i.e., the law-of-the-wall parameters.

In keeping with the fluid mechanics viewpoint, the major effort has been in the determination of velocity profiles so that the radial zone affected by the non-Newtonian properties might be located. As measurements of elastico-viscous flow in the linear sublayer zone have not been made previously, it must be expected that these results are subject to a certain amount of error and further verification. It is not the intention of this report to present conclusive solutions, but rather to clarify the problem and single out the areas for further study.

FLUID CHARACTERISTICS

Additive Selection

At the conception of these tests, the fluid property responsible for the large shear reduction was not known, although there were indications that this property was not the non-linear, shear stress-shear rate relationship. Therefore, the test fluid was selected on the basis of its linearity. If a fluid could be found

which had a linear viscosity and yet reduced the turbulent skin friction, then the property causing the skin friction reduction must be a property other than viscosity.

Six fluids were examined to determine their viscosity, turbulent shear reduction ability and relative deterioration time. Since the facility used was of the recirculating type, fluid deterioration was an important criterion in fluid selection. The fluid viscosity for the selection of the additive was measured on the Fann Model 35 rotational viscometer using rotors of two different diameters. Reduction in turbulent skin friction was determined by subjecting the fluid to the shear produced by an enclosed rotating disc, and observing the power required to turn the constant RPM motor to which the disc was fixed. Degradation of fluid properties was observed by measuring the viscosity and shear reduction as a function of time.

The fluids tested were 0.05% solutions of the following additives:

1. Jaguar - basically a galactomannan which consists of a high molecular weight, carbohydrate polymer having galactose branches; a product of the Stein Hall Company.

2. CMC 7 HSP - a high molecular weight cellulose gum of sodium carboxymethylcellulose; a product of the Hercules Powder Co.

3. J-2P - a guar gum derivative similar to Jaguar but it has preservatives added to inhibit degradation; a product of Westco Research, a division of the Western Company.

4. Reten 205M - a strongly cationic high molecular weight synthetic polymer; a product of the Hercules Powder Company.

5. Natrasol 250 HHR - a cellulose gum similar to CMC but it is nonionic and has a hydration inhibiter; a product of the Hercules Powder Company.

6. Polyox N3000 - a water-soluble resin made from ethylene oxide polymers; a product of the Union Carbide Corp.

The results of the degradation tests performed with domestic water indicated that CMC degraded less than J-2P which, in turn, was more stable than any of the other solutions tested. The viscosity comparisons indicated that the J-2P and CMC solutions also had a viscosity index "n" which was closer to 1.0. As the CMC solution degrades, it's index rapidly approaches 1.0. Although the CMC is slightly more non-linear than the J-2P ($n = 0.95$ for the J-2P as opposed to 0.93 for the CMC) as determined from the viscosity tests, the CMC goes into a true solution while the J-2P forms a suspension only. For these reasons, the CMC was chosen as the additive to be used. CMC is also non-associating, free draining, random coiling and slightly anionic in dilute solutions (14). In addition, CMC has the following characteristics: widely

used in the chemical industry, physiologically inert, easily soluble in water and stable in dry storage. It is synthesized by reacting a well purified cellulose that has first been alkali treated with sodium monochloroacetate. The CMC 7 HSP used has a substitution of only 0.65 to 0.95 (of a possible 3) sodium carboxymethyl groups per anhydro glucose unit. The S in the additive designation means that it has been developed to give thixotropy free solutions.

Mixing and Handling

Since CMC is hydroscopic (equilibrium moisture content at 77°F and 50% relative humidity is 18%), great care was taken to maintain the moisture content constant from its determination to the weighing of the additive immediately before mixing. There are two steps in the mixing of the CMC additives with water. First, the powder is dispersed in the fluid so that it will present the largest possible surface area for hydration. Second, the additive is allowed to hydrate and swell as it goes into solution with the water. If step one is improperly carried out, a lumpy, insoluble mass ensues that has unhydrated CMC in the center. The method for dispersion used in the tests was to pour the powder onto a fine mesh screen where it was broken into a dust. Then this dust was sprinkled into the vortex formed by discharging the system pump into a 55 gallon drum which was mounted inside the 400 gallon reservoir and allowing the overflow to fall into the reservoir. This method worked efficiently throughout the tests and allowed a 400 gallon solution to

be mixed in a few minutes. The volume of the domestic water was determined from the flowmeters used in the test.

Properties

Since there was no method by which the elastic properties could be determined at the low concentrations used, only the viscosity was measured. This viscosity was found to be slightly non-linear and is characterized in this report using the power law approximation. It must be pointed out that this approximation does not include either the normal stresses or elasticity thought necessary to describe the CMC properties completely, but it is the best available.

The Fann Model 35 concentric cylinder, rotational viscometer was used to monitor the fluid viscosity at the test site throughout the experiments. These measurements were used in the reduction of all the experimental results. The Fann viscometer, which has a usable shear rate range from 542 to 3252 sec^{-1}, was calibrated throughout the tests with water. The narrow shear rate range necessitated a different viscometer to check the non-linearity of the viscosity at the higher shear rates experienced in the tests. The Merrill Brookfield High Shear viscometer was used to extend the shear rate range investigated to 70,000 sec^{-1} (shear rate at which parallel flow breaks down). As shown in Figure 1, the power law relation is valid up to the maximum shear rate at which the shear stress is accurate. Although the maximum shear rate used in

the determination of viscosity is less than that produced in the pipe, experimental evidence indicates that for dilute concentrations of some polymer additives, the power law is still valid for shear rates up to 325,000 sec^{-1} (15).

In general, the power law character of the viscosity makes it more imperative to account for the variation of shear rate with radius in the viscometer measurements (1, 16). In all instances with the rotor-stator combination used in the Fann viscometer, this variation was neglected, since the shear rate determined from the angular velocity of the outer cylinder deviated less than 1/3 of 1% from the true shear rate. In the Merrill Brookfield viscometer, the deviation was even less and was also neglected.

Figure 1 also shows the relatively small temperature dependence of the dilute solutions used. In most instances, the temperature of the fluid when tested in the Fann viscometer was different from that at which the pipe flow experiment was run. However, the viscosity variation for the small temperature differences present was interpolated linearly with temperature, and it is believed that the error in this method was negligible compared to the accuracy ($\pm$ 2%) of the overall viscosity determination. Others (17) have noted that 30°F temperature differences in the turbulent flow of dilute CMC solutions have relatively small influence on the shearing resistance.

Degradation of the fluid properties was noted throughout the tube flow experiments. This degradation appears to be both shear and time dependent. New solutions were mixed whenever the power law exponent varied by more than 2% from one run to another. The coefficient, a, in the power law viscosity relation was not controlled, however, and was allowed to vary. This arrangement allowed the same solution to be used as many as three days without change. The variation in the viscosity coefficient with time between test fluid samples was assumed to be linear and accounted for by interpolation of the typical data presented in Figure 2. While a varied between 3.77×10^{-5} and 5.22×10^{-5}, n varied between 0.93 and 0.95. The actual values of a and n corrected for temperature and degradation are shown in the tabulated velocity profiles.

EXPERIMENTAL APPARATUS AND TEST PROCEDURES

Facility

The facility shown in Figure 3 is essentially a closed loop system with a stilling tank and flexible hose feeder added to provide smooth, surge-free flow. In order to eliminate any irregularities, the two test sections (0.650" I.D. and 1.427" I.D.)were polished smooth at the start and periodically during the tests. Fully developed turbulent pipe flow of the non-Newtonian fluid was assured by having 140 pipe diameters upstream of the test section. The two pressure manometers (a 10" null balance micromanometer and

a 6' mercury water U-tube) could be connected across any two of the static pressure taps to provide a check of the pressure drops measured. The checks with water in both pipes at the start of the tests and with CMC in the small pipe throughout the tests indicated no systematic differences between the pressure taps. During the experiments in the large pipe, two sets of pressure taps became inoperative due to the chemical attack of the CMC on the aluminum clad tubing, and prevented a check of the pressure data in that pipe. Three flowmeters were required to cover the desired range of flow rates: a 300 gal./min. Smith totaling flowmeter, a 60 gal./min. Smith totaling flowmeter, and a 3/8" Pottermeter ($1\frac{1}{2}$ to 4 gal./min.). These flowmeters were believed accurate within $\pm$ 2% by previous calibration with oil. Cooling coils were installed in the storage tank to maintain the test fluid temperature throughout a series of runs. Fluid temperature was measured both in the storage tank and at the end of the $2\frac{1}{2}$-inch feeder line.

Instrumentation

In order to measure velocities inside the sublayer, a probe of small dimensions was needed. This probe consisted of five telescoping stainless steel tubes as shown in Figure 4. The probe tip was formed by inserting a copper wire in the stainless steel tubing, heating the tubing to a cherry red temperature and then hammering the tube flat. After etching out the copper wire with sulfuric acid, the tubing was ground to the proper dimension. The radial

position of the probe tip in the pipe was indicated by a depth micrometer which measured the displacement of the probe tip from the point where it made electrical contact with the wall. The overall error in the determination of the probe position is believed to be less than 0.0005 inches. The measurement errors due to velocity gradient, wall interference, turbulence and static pressure tap location will be discussed later.

A differential pressure transducer was used to determine the dynamic pressure in order to reduce the time to take the velocity readings; the response time was decreased by a factor of 4000 in using a pressure transducer instead of a $\frac{1}{4}$-inch U-tube water-oil manometer. The pressure transducers were calibrated using a micromanometer having .0002 inches of water sensitivity and a secondary standard mercury manometer. The output of the pressure transducer was first amplified by a CEC carrier system,then by a Kintel DC amplifier, and the system output was displayed on a Hewlett Packard 1 MV, three place digital voltmeter. By calibrating the transducer over several decade ranges, adjusting the gain in each of these ranges to give a 1000 mV output and using high accuracy manometers for calibration, the overall error in the instrumentation system was determined to be less than $\pm$ 3/4%. Several capacitors were used in the output circuit to eliminate fluctuations in the pressure readings.

Test Procedures

Since the most important measurements were of fluid velocity, the experimental procedure was designed to minimize any errors which might be present in the velocity instrumentation. After first adjusting the flow rate to the desired value and allowing the fluid temperature to stabilize, the facility was shut down and the zero differential pressure on the transducer was read. Then the flow was started and allowed to stabilize before an electrical indication of the wall position was made. The velocity profile, pressure drop, flow rate, and temperature were then measured simultaneously. If there were any appreciable differences in any of the last three of the above quantities,the run was discarded and repeated at a later time. The viscosity was measured after every four hours of running, and the fluid viscosity at intermediate times was interpolated linearly from these data.

RESULTS AND DISCUSSION

There have been several experimental programs performed previously (3, 4, 17) to determine the turbulent and laminar flow characteristics of more concentrated CMC solutions. The large differences in fluid properties, however, prevent any close comparisons of experimental results. Even in instances where the same concentrations of a single polymer additive are used, the fluid viscosity is most often different and dependent upon the solvent purity (18).

In addition, the fluid elasticity may be affected by the solvent purity in a manner that is different from that of the viscosity. Also, since the effects of tube diameter are unknown, no comparisons can be made between data taken in tubes of different sizes. These effects have prevented the cross checking of experimental results,and for this reason,all of the data reported herein are for a single fluid viscosity index within experimental limitations.

Basically, the problem of specifying the correlation of the turbulent friction factor with the Reynolds number resolves itself into two dependent parts: first, the determination of the complete relation between shear stress and shear rate; second, the determination of velocity as a function of radial position in terms of universal constants. Universal constants are those which can be determined experimentally and can be applied to a physical boundary layer flow field independent of fluid type, free stream velocity, and surface geometry. These two processes will now be considered in detail.

At present, the fluid properties that can be measured are incomplete since they neglect elasticity, and the power law relation used is, at best, only an approximation for the viscous properties. However, this viscosity characterization worked reasonably well for friction factor prediction in laminar flow (5) and therefore was extended to turbulent flow. In addition, the power law was used to change several parameters in the universal velocity correlation,

$u/u^* = A \log_{10} u^*y/\nu + D$, known as the law of the wall, which was expected to predict the correct velocity profiles. Since the power law viscosity changes with radial distance (shear rate), in the past it was thought necessary to account for this effect in all the turbulent velocity correlations (4,19,20). This changed the usual parameter for the radial change of velocity, yu^*/ν, to $\rho\, y^n u_*^{2-n}/a$, which made the theoretical velocity gradient vary as a function of n. However, in turbulent flow, viscosity is most important at the wall and serves as a reference parameter only for the remaining velocity field since the momentum is transferred through the fluid by a macroscopic process rather than a microscopic process. Therefore the usual "law-of-the-wall" parameters were used with only the viscosity modified, as shown below.

The original formulation of the law-of-the-wall was based on experimental observations in a pipe, dimensional analysis, and the formulation of some simple similarity laws (21). This formulation is based on the shear velocity, $u^{*2} = \tau_w/\rho$, at the wall and to be consistent within the assumption of the similarity laws, the viscosity must also be determined at the wall. Therefore, defining

$$\upsilon_w = \frac{\tau_w}{\rho(du/dy)_w} \tag{2}$$

and assuming that the power law applies at the wall

$$\tau_w = a\left(\frac{du}{dy}\right)_w^n$$

we have, after substitution, that

$$\upsilon_w = \frac{\tau_w^{1-1/n} \; a^{1/n}}{\rho} ,$$

This value of viscosity at the wall was used in the reduction of all the velocity data to the universal form.

Using the universal velocity correlations with the constants A and D determined experimentally, Prandtl (22) found it was possible to derive the friction factor versus Reynolds number relationship. Nikuradse (23), by using his experimental results to modify slightly the constants derived for this relation, predicted all the experimental data up to a Reynolds number of 3×10^6. This relation is used later for the comparison of experimental data with Newtonian theory.

Although a new Reynolds number could be based on the υ_w, at the present it is better for two reasons to continue with the existing power law Reynolds number, $R_n = 8[2\ (3+1/n)]^{-n}\ [\rho d^n\ \bar{u}^{2-n}/a]$, derived from laminar flow considerations (5). First, all of the previous experimental data have been presented and compared on this basis and a different Reynolds number would only increase the present confusion of experimental results. Second, the υ_w presupposes knowledge of the τ_w which is the quantity that the correlation should predict. Therefore, the universal velocity data will be presented in terms of υ_w, while the friction factor vs. Reynolds number data will be presented in terms of R_n.

Velocity Measurements

As mentioned previously, the velocity data is subject to four errors of measurement and each of these will be considered before discussing the velocity results. At low probe Reynolds numbers, the viscous action of the fluid increases the stagnation point pressure and a total pressure probe gives a false indication of the stagnation pressure. At the lowest velocity used in these tests, the tip Reynolds number based on the probe tip height is approximately 50 which makes the velocity indicated by the probe approxmately 0.5 percent low (24). The effect of the large velocity gradients close to the wall is to displace the point at which the true stagnation pressure is measured away from the wall (25). This phenomenon serves to increase the velocity actually measured. For the probe dimensions used, the effective center of the probe should be displaced by approximately 0.001 inch. The expected turbulence level also serves to increase the dynamic pressure measured at the probe tip, thereby increasing the velocity slightly (26). Finite static tap diameter increases the static pressure (27,28) and thus reduces the measured velocity by less than 0.5 percent. Overall, the expected probe and tap diameter effects would tend to decrease the integrated flow rates by less than 0.5 percent while the velocity close to the wall would be increased slightly.

The forementioned results are based on experimental results obtained from measurements on Newtonian fluids. In particular,

most of the possible effective center corrections have been justified by agreement with the hypothesized linear sublayer, but no such hypothesis has been demonstrated experimentally for non-Newtonian fluids. Therefore, it was decided not to make any adjustment of the data and present the original data for individual interpretation.

All of the velocity data* is presented in terms of the turbulent boundary layer parameters of Φ and η. The solid line on each plot is the empirical expression for the turbulent Newtonian flow of fluids proposed by J. D. Coles (29), $\Phi = 5.75 \log_{10} \eta + 4.5$. Figure 5 shows a typical profile for water. As none of the corrections discussed earlier have been made, there is a tendency for the displacement of the probes effective center away from the wall to indicate a greater velocity than that actually present. A displacement of the effective center by only 0.002 inch would give excellent agreement between the velocity profile and the empirical curve. Figures 6 through 12 and 13 through 18 present the results of the measurement of turbulent velocity profiles of 0.05% CMC in the small pipe and large pipe respectively. The Φ , η relationship is based on the assumption that there are three different regions of flow as indicated by the curve. For $\eta > 30$, the flow is fully turbulent and the effect of viscosity is negligible. For $\eta < 8$, the flow is essentially linear and viscosity predominates. The

---

* Tabulated velocity profiles are included in Appendix I.

third region is a buffer zone between the other two.

Looking first at the fully turbulent region, the most significant effect is the parallel shift of the velocity by as much as 28% at the highest R_n. From the phenomenological point of view, the parallel shift means that the mixing length remains unchanged by the elastico-viscous properties of the fluid since the coefficient of $\log_{10} \eta$ is dependent on the mixing length. This shift indicates that a fluid property in addition to viscosity is needed to correlate the data if the mixing length concept is correct. Also, since the magnitude of the shift is dependent on R_n, any correlating parameter must be a function of the flow field as well.

When a plot is made in terms of the velocity defect law, $(u_m - u)/ u^* = f(2y/d)$, the 0.05% CMC solutions agree well with the empirical relationship for Newtonian fluids. This is to be expected since the mixing length parameter, k, is unchanged.

From a physical point of view, the constant slope with increasing R_n implies that the mechanism of turbulent momentum transport remains the same and is independent of R_n. The decrease in magnitude of the turbulent mixing as reported by Metzner (4) must then have only a small effect on the rates of momentum transport at these small concentrations.

The velocity profiles for the small pipe will be examined first for overall trends since this set of data has both the greatest

R_n range and accuracy. The linear region close to the wall displays no deviation from that expected for Newtonian fluids at low R_n. Actually, at $R_n = 1.33 \times 10^4$, Figure 7, the velocity data, which is uncorrected for displacement of effective center, shows a better agreement with the Newtonian correlation than the uncorrected zero concentration measurements, implying that the net velocity correction may be smaller for elastico-viscous fluids. If one looks closely at the region between $\eta = 8$ and $\eta = 30$ in Figures 8, 9 and 10, it appears that the velocity in the buffer zone is uniformly displaced in proportion to that in the fully turbulent region. This somewhat unexpected result would seem to indicate that the significant effect of the elastico-viscous fluid properties is felt in the linear sublayer next to the wall. If one hypothesizes that the linear sublayer remains unchanged by the elastico-viscous properties, then the velocity in the buffer zone should become asymptotic to the linear sublayer velocity at small η. This did not happen as shown above and there could be several reasons why it did not. First, the velocity indicated by the probe may be incorrect. Second, the major elastico-viscous effect may truly be in the linear sublayer. There is much evidence (30) to suggest that the linear sublayer is not laminar at all but is composed of longitudinal and transverse oscillations close to the wall. If this were true, it might explain why the steady laminar flow fields of elastico-viscous fluids can be predicted, and the

linear sublayer flow fields of turbulent flow at higher Reynolds numbers cannot.

The remaining figures for the small pipe show a continuing increase in the upward displacement of the velocity profile. There is no indication from the available data that this increasing displacement will not continue for even larger R_n.

The large pipe shows much the same effect; however, the data is over a more limited range (Figs. 13 through 18). At $R_n = 9.80 \times 10^4$, Figure 14, the same uniform displacement of the velocity profile in the buffer region is noted.

When the constant, D, in the law-of-the-wall relationship for the two pipe sizes is compared versus R_n, as in Figure 19, the differences between the flow in the different sized pipes can readily be seen. The differences correspond exactly with that which is observed in the f vs R_n correlation, since the friction factor is an inverse function of D. At high R_n, the friction factor for the small pipe is less than that of the large pipe, while at low R_n, the opposite is true. Based on Figure 19, it is easy enough to predict what will happen in these sizes of pipe with this particular fluid but such a correlation, without additional data, would be useless for extrapolation to other fluid concentrations or pipe sizes, and is therefore omitted.

The velocity profiles obtained show no agreement with the semi-theoretical results predicted by Granville, Dodge and Metzner, and

Clapp for power law fluids, thereby indicating again the presence of elasticity or some additional property other than a non-linear viscosity.

Friction Factor Measurements

Shown in Figure 20 is the experimental determination of the friction factor versus R_n correlation for both water and 0.05% CMC solutions for the small pipe. The Reynolds number for the test runs with water were determined from the flowmeter readings since there were no velocity profiles taken. All of the data with CMC was based on the integrated velocity profiles, since these profiles were considered the most reliable piece of information taken from the tests. A typical plot from which the integrated flow rate was taken is shown in Figure 21. Except for several very low flow rates on the 3/8 Pottermeter which were discarded, all of the integrated profiles showed an average increase in flow rate 7% greater than that indicated by the flowmeters. This effect is as yet unexplained but it is interesting to note that others (17) using a different type of flowmeter and higher concentrations have observed the same variation. The maximum reduction in skin friction ($\approx$ 48%) is observed at the highest Reynolds number in the small pipe. Although this reduction in skin friction is not insignificant, it is small compared to what is usually obtained at higher concentrations. However, the purpose of this study was to obtain a liquid having a power law index, n, as close to one (Newtonian) as possible

in order to separate elastic effects from viscous effects. It is interesting to note that at $R_n = 6 \times 10^3$, there appears to be an increase in friction factor for the non-Newtonian fluid. Although the overall error of the friction factor-Reynolds numbers determination is believed to be less than $\pm$ 2%, at this low flow rate, 1.4 gal./min., the experimental error may account for the increase. None of the existing power law turbulent flow correlations predict the curve measured. There does not appear to be any appreciable increase in the transition Reynolds number even though the data does not completely cover this range.

In the large pipe, the difficulties with the pressure taps required a more careful scrutiny of both the water and CMC data. As shown in Figure 22, the friction factors for water were determined both at the beginning of the tests and at the end, and either from the flowmeter or from the integrated velocity profiles. It is obvious from this water data that the CMC has had an adverse effect on the accuracy of the pressure drops indicated. For this reason, it was decided to use the pressure drop data for the CMC taken early in the tests (when there was good agreement between the experimental and empirical friction factors for water) in combination with a separate set of integrated velocity profiles taken later in the tests to determine the friction factors used for the 0.05% CMC solutions in the large pipe. A best fit straight line through the large pipe CMC data would be more parallel to the Newtonian curve

and intersect at a lower Reynolds number than a similar line drawn through the small pipe data.

CONCLUSIONS

The following conclusions may be drawn from the experimental data presented:

1. The decrease in friction factor from the Newtonian value with decreasing pipe diameter is as reported experimentally elsewhere.

2. For the low CMC concentrations used, the friction factor indicates no large increase in the Reynolds number for transition.

3. The major effect of the CMC solutions is a shift linearly upward (increasing with R_n) of the velocity parameter in the universal law of the wall relationship. This indicates that the mixing length constant has not been affected by the elastico-viscous properties.

4. The lack of agreement with the correlations proposed for pseudo-plastic or power law fluids indicates that there is an additional property required to fully describe its motion.

ACKNOWLEDGEMENT

The work reported here is part of a project supported jointly by independent research and development funds of Ling-Temco-Vought, Inc., and the National Aeronautics and Space Administration under Contract No. NASw-729.

NOTATION

a	non-Newtonian fluid property, defined by Eq. (1)
A	dimensionless constant in universal velocity correlation
C	concentration, percent by weight
d	pipe diameter
D	dimensionless constant in universal velocity correlation
f	friction factor, $2\ \tau_w/\rho\ \bar{u}^2$
n	non-Newtonian fluid index, defined by Eq. (1)
Q	flow rate
r	radial coordinate, distance from the tube centerline
R_n	power law Reynolds number
u	velocity in the x-direction
$\bar{u}$	bulk velocity $(4Q/\pi d^2)$
u_*	friction velocity $(\tau_w/\rho)^{\frac{1}{2}}$
y	normal coordinate, distance from the wall

Greek letters

τ_w	shear stress at the wall
ρ	density

ϕ non-dimensional velocity (u/u_*)

η non-dimensional normal coordinate (yu_*/υ_w)

υ viscosity

υ_w viscosity, defined by Eq. (2)

LITERATURE CITED

1. Wilkinson, W. L., Non-Newtonian Fluids, Pergamon Press, N.Y. (1960).
2. Metzner, A. B., Handbook of Fluid Dynamics, Chapter 7, McGraw Hill, N.Y. (1961).
3. Shaver, R. G., and Merrill, E. W., A.I.Ch.E. Journal, 5, 181 (1959)
4. Dodge, D. W., and Metzner, A. B., A.I.Ch.E. Journal, 5, 189 (1959).
5. Metzner, A. B., and Reed, J. C., A.I.Ch.E. Journal, 1, 435 (1955).
6. Oldroyd, J. G., Proc. Roy. Soc. (London), Ser. A245, 278 (1958).
7. Walters, K., Quart. J. Mech. and Appl. Math., 15, 63 (1962).
8. Rivlin, R. S., and Ericksen, J. L., J. Rational Mech. Anal., 4, 323 (1955).
9. Coleman, B. D., and Noll, W., Ann. N. Y. Acad. Sci., 89, 672 (1961).
10. Rivlin, R. S., J. Rational Mech. Anal., 4, 681 (1953).
11. Truesdell, C., Trans. Soc. Rheo., 4, 9 (1960).
12. Metzner, A. B., speech at the American Physical Society Meeting, Boston, (November, 1963).

13. Wells, C. S., Am. Inst. Aero. Astro. Preprint No. 64-36 (1964).

14. Anon. Hercules Cellulose Gum - Properties and Use, Hercules Powder Co., Wilmington, Delaware (1960).

15. Crawford, H. R., private communication to the author.

16. Savins, J. G., private communication to the author.

17. Ripkin, J. F., and Pilch, M., St. Anthony Falls Hydraulic Laboratory, Technical Paper 42, Series B (1963).

18. Ernst, W. D., LTV Research Center Report No. 0-71000/5R-2 (1965).

19. Clapp, R. M., International Developments in Heat Transfer, 3, 652 (1961).

20. Granville, P. S., David Taylor Model Basin Report 1579 (1962).

21. Schlichting, H., Boundary Layer Theory, McGraw Hill, New York (1960).

22. Prandtl, L., Aerodynamic Theory, III, 142 (1935).

23. Nikuradse, J., VDI Forschungsheft, 356, (1932).

24. MacMillan, F. A., J. Roy. Aero. Soc., 58, 837 (1954).

25. Young, A. D., and Maas, J. N., Aero. Res. Comm. R & M 1770 (1936).

26. Goldstein, S., Proc. Roy. Soc. (London), Ser. A155, 570 (1936).

27. Shaw, R., J. Fluid Mech., 7, 550 (1960).

28. Rayle, R. E., SM Thesis, Mass. Inst. of Technol. (1949).

29. Coles, D., Ph.D. Thesis, Cal. Inst. Technol. (1953).

30. Sternberg, J., J. Fluid Mech., 13, 241 (1962).

31. Hodgman, C. D., ed., "Handbook of Chemistry and Physics, 32 ed., p 1827 (1950).

APPENDIX I

TABLE 1 THROUGH TABLE 13

TABULATION OF VELOCITY PROFILES

TABLE I

See Figure 6

$\mathbb{R}_n = 6.012 \times 10^3$

$d = 0.0542$

$a = 3.770 \times 10^{-5}$

$n = 0.950$

$\bar{u} = 1.66$

$\upsilon_w = 1.373 \times 10^{-5}$

$u_* = 0.1170$

y [Inches]	u [ft./sec.]
.0030	.416
.0035	.440
.0040	.507
.0045	.463
.0050	.493
.0055	.515
.0060	.606
.0065	.588
.0075	.623
.0085	.699
.0095	.728
.0115	.851
.0135	.914
.0155	.988
.0175	1.078
.0215	1.238
.0255	1.261
.0355	1.462
.0455	1.520
.0655	1.689
.0855	1.726
.1225	1.849
.1725	1.940
.2225	2.02
.2725	2.064
.3225	2.080

TABLE II

See Figure 7

$\mathbb{R}_n = 1.327 \times 10^4$

$d = 0.0542$

$a = 3.747 \times 10^{-5}$

$n = 0.950$

$\bar{u} = 3.50$

$\upsilon_w = 1.282 \times 10^{-5}$

$u_* = 0.2104$

y [Inches]	u [ft./sec.]
.0030	.863
.0035	.633
.0040	.828
.0045	1.170
.0050	1.284
.0055	1.490
.0060	1.599
.0065	1.704
.0075	1.750
.0085	1.992
.0095	2.091
.0115	2.481
.0135	2.656
.0155	2.522
.0175	2.656
.0215	2.875
.0255	3.055
.0355	3.125
.0455	3.295
.0655	3.488
.0855	3.585
.1225	3.785
.1725	4.09
.2225	4.31
.2725	4.449
.3225	4.513

TABLE III

See Figure 8

$\mathbb{R}_n = 3.183 \times 10^4$

$d = 0.0542$

$a = 4.401 \times 10^{-5}$

$n = 0.941$

$\bar{u} = 8.82$

$\upsilon_w = 1.285 \times 10^{-5}$

$u_* = 0.4331$

y [Inches]	u [ft./sec.]
.0030	5.36
.0035	5.47
.0040	5.64
.0045	5.89
.0050	6.04
.0055	6.145
.0060	6.34
.0065	6.43
.0075	6.76
.0085	6.88
.0095	6.95
.0115	7.17
.0135	7.29
.0155	7.385
.0175	7.48
.0215	7.60
.0255	7.78
.0355	7.98
.0455	8.25
.0655	8.60
.0855	8.98
.1225	9.32
.1725	9.85
.2225	10.15
.2725	10.46
.3225	10.59

TABLE IV

See Figure 9

$\mathbb{R}_n = 6.991 \times 10^4$

$d = 0.0542$

$a = 4.428 \times 10^{-5}$

$n = 0.941$

$\bar{u} = 18.6$

$\nu_w = 1.197 \times 10^{-5}$

$u_* = 0.796$

y [Inches]	u [ft./sec.]
.0030	12.71
.0035	12.59
.0040	13.01
.0045	13.46
.0050	13.61
.0055	13.98
.0060	14.29
.0065	14.49
.0075	14.78
.0085	14.78
.0095	15.23
.0115	15.42
.0135	15.62
.0155	15.91
.0175	16.11
.0215	16.39
.0255	16.63
.0355	17.17
.0455	17.62
.0655	18.09
.0855	18.90
.1225	19.71
.1725	20.70
.2225	21.48
.2725	21.99
.3225	22.21

TABLE V

See Figure 10

$\mathbb{R}_n = 1.128 \times 10^5$

$d = 0.0542$

$a = 4.510 \times 10^{-5}$

$n = 0.941$

$\bar{u} = 29.7$

$\nu_w = 1.167 \times 10^{-5}$

$u_* = 1.15$

y [Inches]	u [ft./sec.]
.0030	20.99
.0035	21.30
.0040	21.93
.0045	22.45
.0050	22.68
.0055	23.09
.0060	23.65
.0065	23.77
.0075	24.14
.0085	24.20
.0095	24.59
.0115	24.92
.0135	25.37
.0155	25.61
.0175	26.01
.0215	26.39
.0255	26.62
.0355	27.60
.0455	28.21
.0655	29.24
.0855	30.37
.1225	31.29
.1725	32.67
.2225	33.65
.2725	34.28
.3225	34.61

TABLE VI

See Figure 11

$\mathbb{R}_n = 1.454 \times 10^{-5}$

$d = 0.0542$

$a = 4.538 \times 10^{-5}$

$n = 0.941$

$\bar{u} = 38.0$

$\nu_w = 1.144 \times 10^{-5}$

$u_* = 1.412$

y [Inches]	u [ft./sec.]
.0030	26.95
.0035	26.85
.0040	27.77
.0045	28.62
.0050	29.16
.0055	29.59
.0060	29.75
.0065	30.25
.0075	30.92
.0085	31.48
.0095	31.75
.0115	32.21
.0135	32.72
.0155	33.03
.0175	33.33
.0215	33.99
.0255	34.50
.0355	35.5
.0455	36.44
.0655	37.6
.0855	38.6
.1225	40.2
.1725	41.6
.2225	42.85
.2725	43.75
.3225	44.05

TABLE VII

See Figure 12

$R_n = 2.105 \times 10^5$

$d = 0.0542$

$a = 4.538 \times 10^{-5}$

$n = 0.941$

$\bar{u} = 53.9$

$\upsilon_w = 1.102 \times 10^{-5}$

$u_* = 1.902$

y [Inches]	u [ft./sec.]
.0030	38.46
.0035	39.99
.0040	40.99
.0045	41.75
.0050	42.50
.0055	42.80
.0060	43.49
.0070	44.00
.0080	44.75
.0090	45.20
.0110	45.99
.0130	46.60
.0150	47.25
.0170	47.77
.0210	48.3
.0250	49.3
.0350	50.76
.0450	52.25
.0650	53.7
.0850	55.1
.1220	57.1
.1720	58.7
.2220	60.35
.2720	61.6
.3220	62.25

TABLE VIII

See Figure 13

$R_n = 4.424 \times 10^4$

$d = 0.1189$

$a = 5.160 \times 10^{-5}$

$n = 0.930$

$\bar{u} = 6.57$

$\upsilon_w = 1.444 \times 10^{-5}$

$u_* = 0.3019$

y [Inches]	u [ft./sec.]
.0030	3.581
.0035	3.619
.0040	3.695
.0045	3.702
.0050	3.748
.0055	3.885
.0060	4.03
.0070	4.24
.0080	4.43
.0100	4.78
.0120	4.92
.0160	5.21
.0200	5.36
.0280	5.57
.0360	5.68
.0560	5.89
.0840	6.13
.1090	6.41
.1340	6.49
.2000	6.89
.2840	7.13
.3590	7.37
.4590	7.59
.5590	7.85
.6590	8.005

TABLE IX

See Figure 14

$R_n = 9.796 \times 10^4$

$d = 0.1189$

$a = 5.127 \times 10^{-5}$

$n = 0.930$

$\bar{u} = 13.7$

$\upsilon_w = 1.297 \times 10^{-5}$

$u_* = 0.592$

y [Inches]	u [ft./sec.]
.0030	8.09
.0035	8.04
.0040	8.32
.0045	8.69
.0050	8.849
.0055	9.085
.0060	9.39
.0070	9.72
.0080	9.85
.0100	10.239
.0120	10.439
.0160	10.61
.0200	11.13
.0280	11.32
.0360	11.531
.0470	12.17
.0840	12.84
.1090	13.31
.2090	14.25
.3590	15.34
.4590	15.89
.5590	16.19
.6490	16.39

TABLE X

See Figure 15

$\mathbb{R}_n = 1.846 \times 10^5$

$d = 0.1189$

$a = 5.127 \times 10^{-5}$

$n = 0.930$

$\bar{u} = 24.8$

$\upsilon_w = 1.211 \times 10^{-5}$

$u_* = 0.931$

y [Inches]	u [ft./sec.]
.0030	15.9
.0035	16.1
.0040	16.1
.0045	16.8
.0050	17.1
.0055	17.7
.0060	18.0
.0070	18.5
.0080	18.6
.0100	19.1
.0120	19.3
.0160	20.0
.0200	20.5
.0280	21.3
.0360	21.6
.0560	22.6
.0840	23.4
.1090	23.9
.1340	24.4
.2090	25.4
.2840	26.4
.3590	27.1
.4590	27.8
.5590	28.4
.6590	28.7

TABLE XI

See Figure 16

$\mathbb{R}_n = 2.575 \times 10^5$

$d = 0.1189$

$a = 5.224 \times 10^{-5}$

$n = 0.930$

$\bar{u} = 34.5$

$\upsilon_w = 1.178 \times 10^{-5}$

$u_* = 1.288$

y [Inches]	u [ft./sec.]
.0030	21.1
.0035	21.5
.0040	22.6
.0045	23.4
.0050	24.2
.0055	24.4
.0065	25.2
.0075	25.4
.0095	26.1
.0115	26.9
.0155	27.5
.0195	28.2
.0275	29.2
.0355	29.9
.0555	31.2
.0835	32.9
.1085	33.4
.1335	34.4
.2085	35.6
.2835	37.0
.3585	37.8
.4585	39.0
.5585	39.5
.6585	39.9

TABLE XII

See Figure 17

$\mathbb{R}_n = 4.524 \times 10^5$

$d = 0.1189$

$a = 5.127 \times 10^{-5}$

$n = 0.930$

$\bar{u} = 57.4$

$\upsilon_w = 1.081 \times 10^{-5}$

$u_* = 1.99$

y [Inches]	u [ft./sec.]
.0030	39.8
.0035	40.3
.0040	41.3
.0045	42.2
.0050	43.1
.0060	43.8
.0070	44.6
.0090	46.0
.0110	46.8
.0150	48.2
.0190	49.1
.0270	50.6
.0350	51.8
.0550	53.7
.0830	55.4
.1080	56.6
.1330	57.7
.2080	59.9
.2830	61.5
.3580	62.9
.4580	64.3
.5580	65.5
.6580	66.1

TABLE XIII

See Figure 18

$\mathbb{R}_n = 4.586 \times 10^5$

$d = 0.1189$

$a = 5.324 \times 10^5$

$n = 0.930$

$\bar{u} = 60.2$

$\upsilon_w = 1.119 \times 10^{-5}$

$u_* = 2.066$

y [Inches]	u [Ft./sec.]
.0033	41.01
.0038	41.30
.0043	41.55
.0048	42.30
.0053	43.40
.0063	44.85
.0073	45.82
.0093	47.15
.0133	49.35
.0173	50.70
.0213	51.62
.0293	52.97
.0453	54.63
.0653	56.20
.0853	57.25
.1363	59.47
.1863	62.22
.2663	63.10
.3413	64.55
.4163	66.06
.4913	67.25
.5663	67.97
.6413	68.62

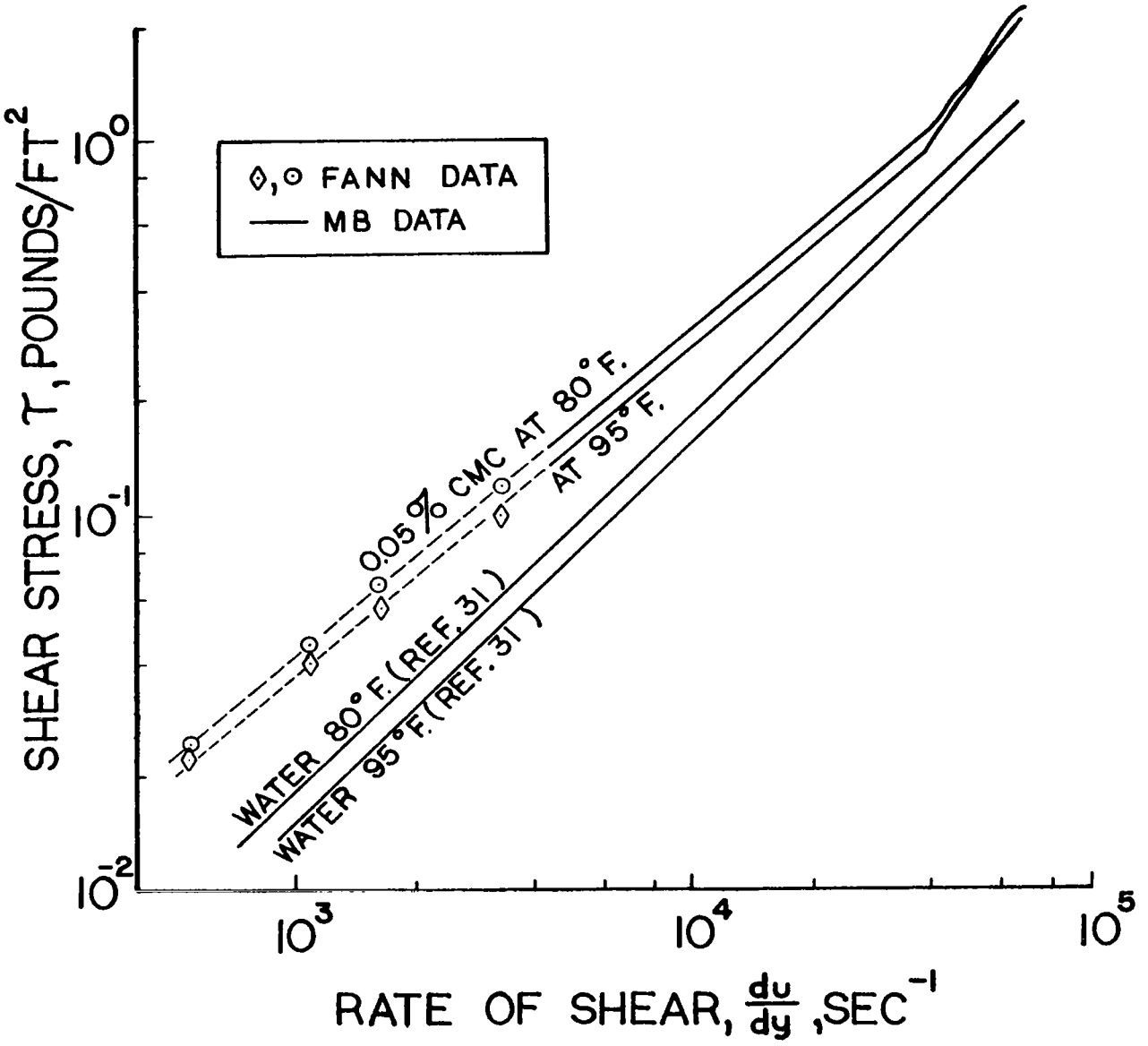

Fig. 1 Comparison of Shear Stress Data Taken in the Fann and Merrill Brookfield Viscometers.

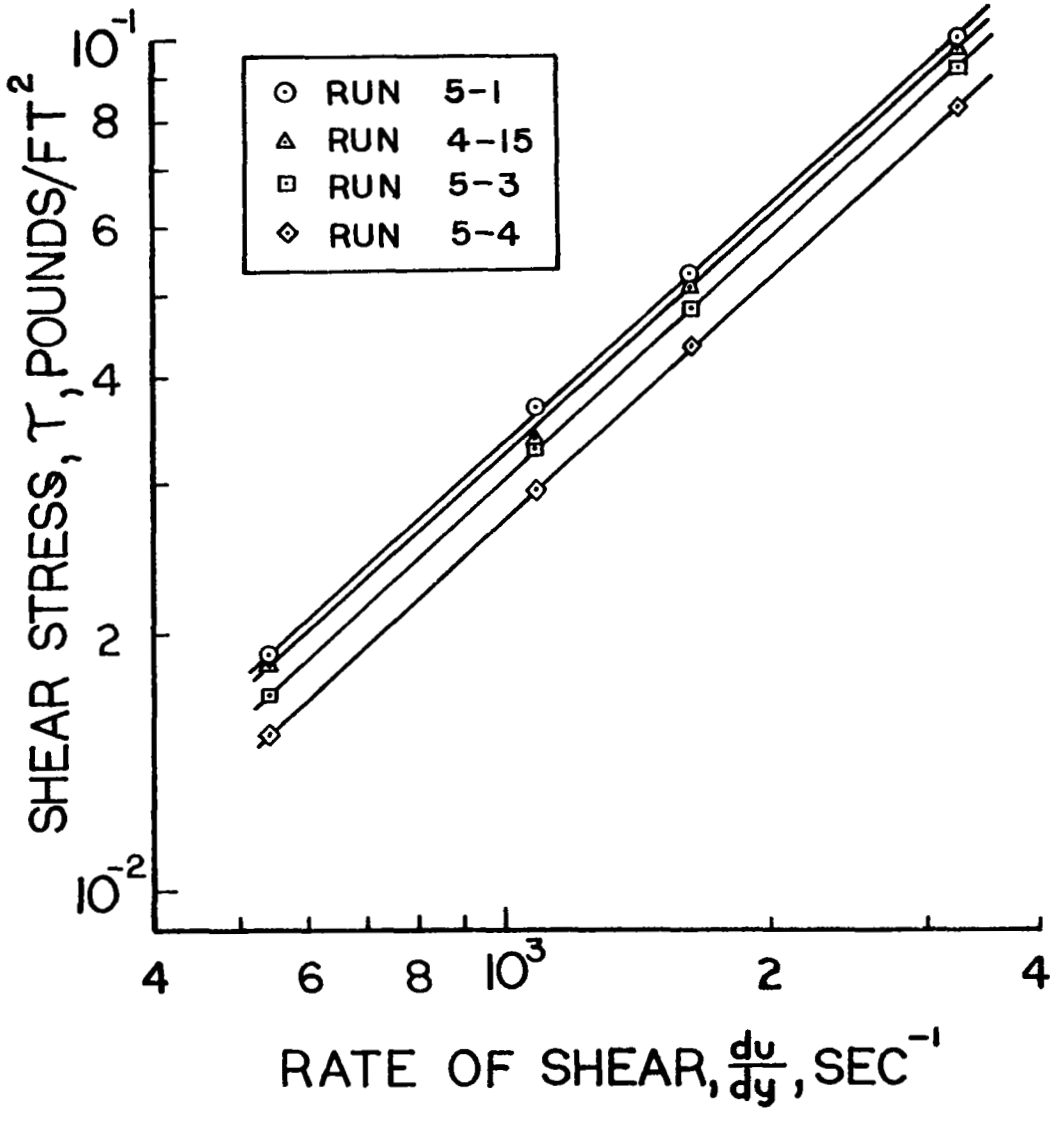

Fig. 2 Typical Low Shear Rate Data for Test Solutions

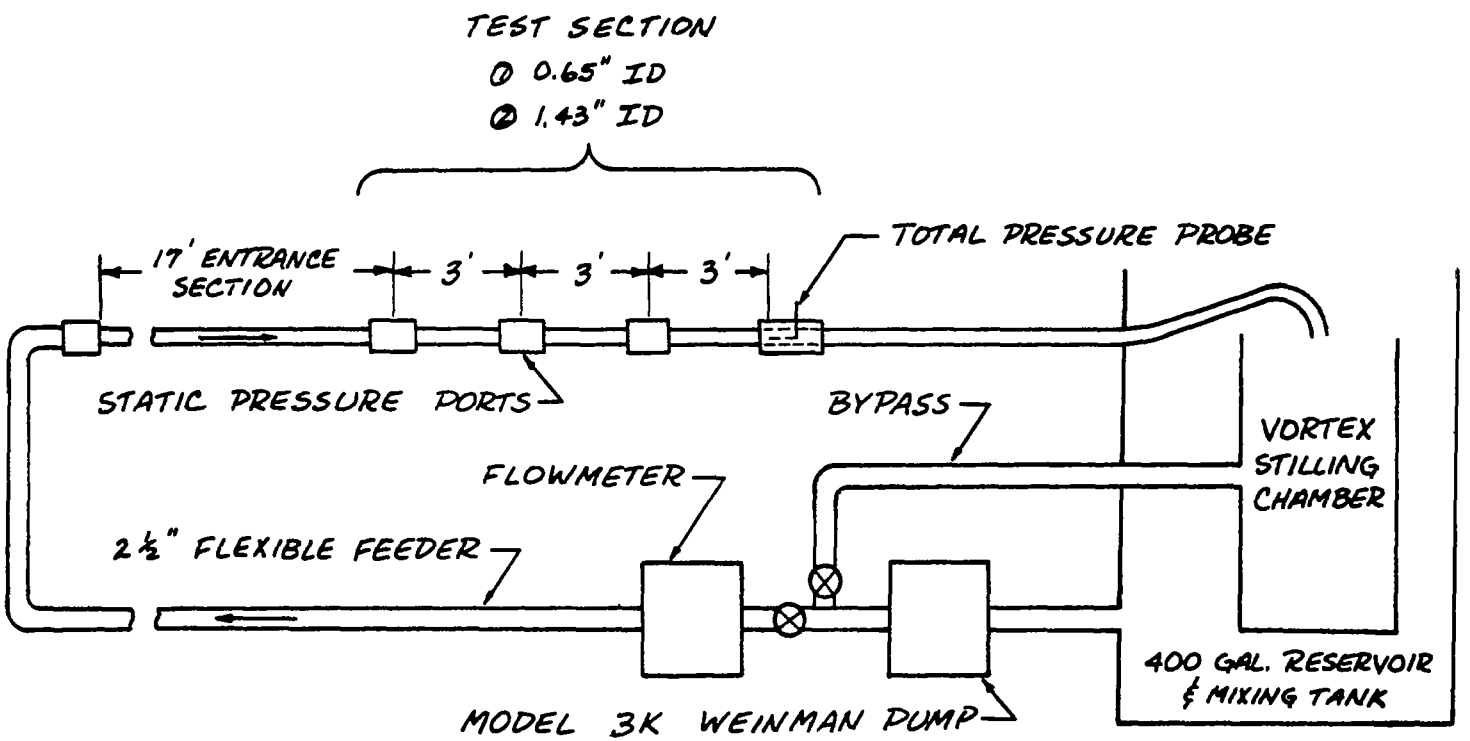

Fig. 3 Schematic of Test Facility

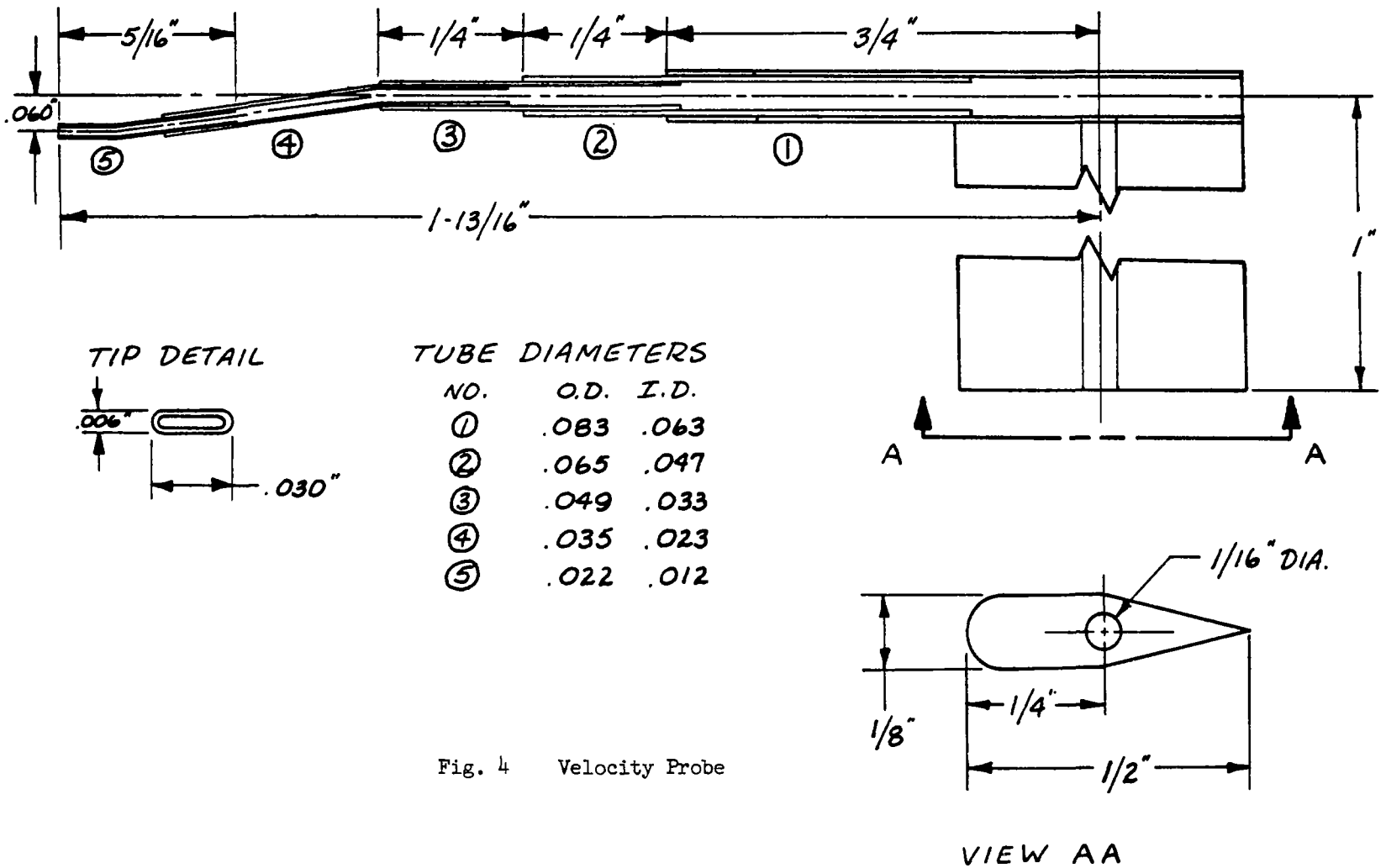

TUBE DIAMETERS

NO.	O.D.	I.D.
1	.083	.063
2	.065	.047
3	.049	.033
4	.035	.023
5	.022	.012

Fig. 4 Velocity Probe

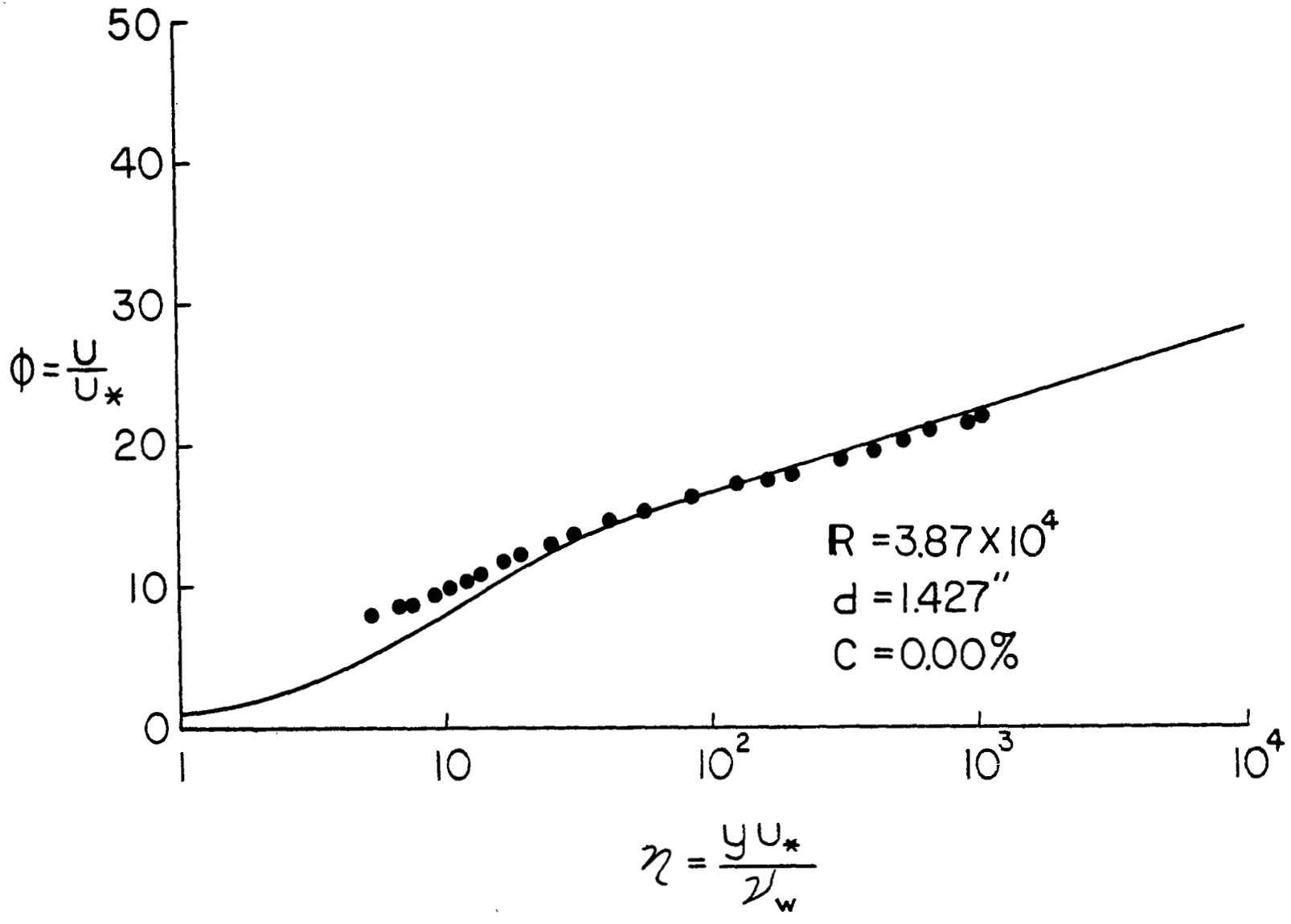

Fig. 5 Generalized Velocity Profile

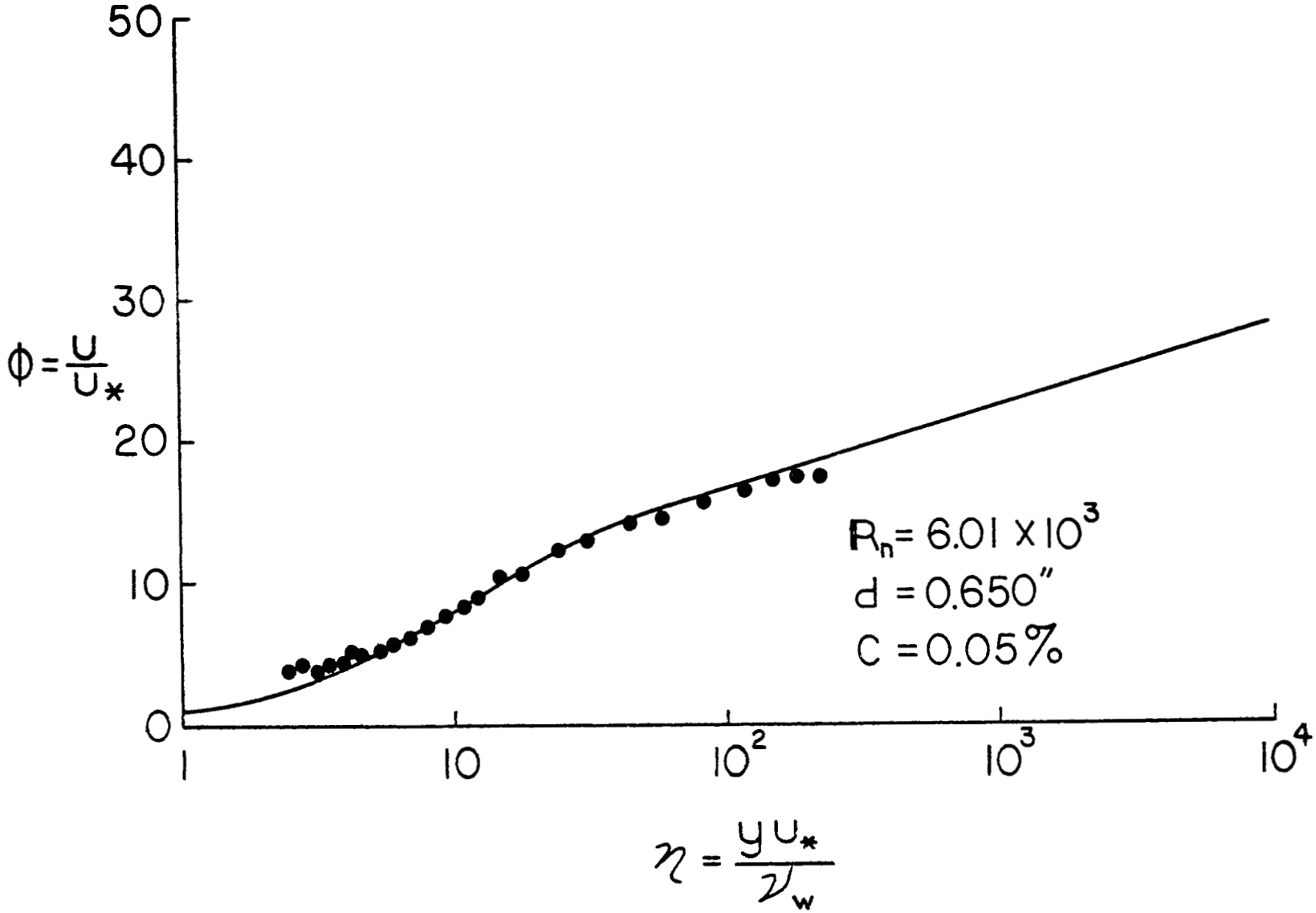

Fig. 6 Generalized Velocity Profile

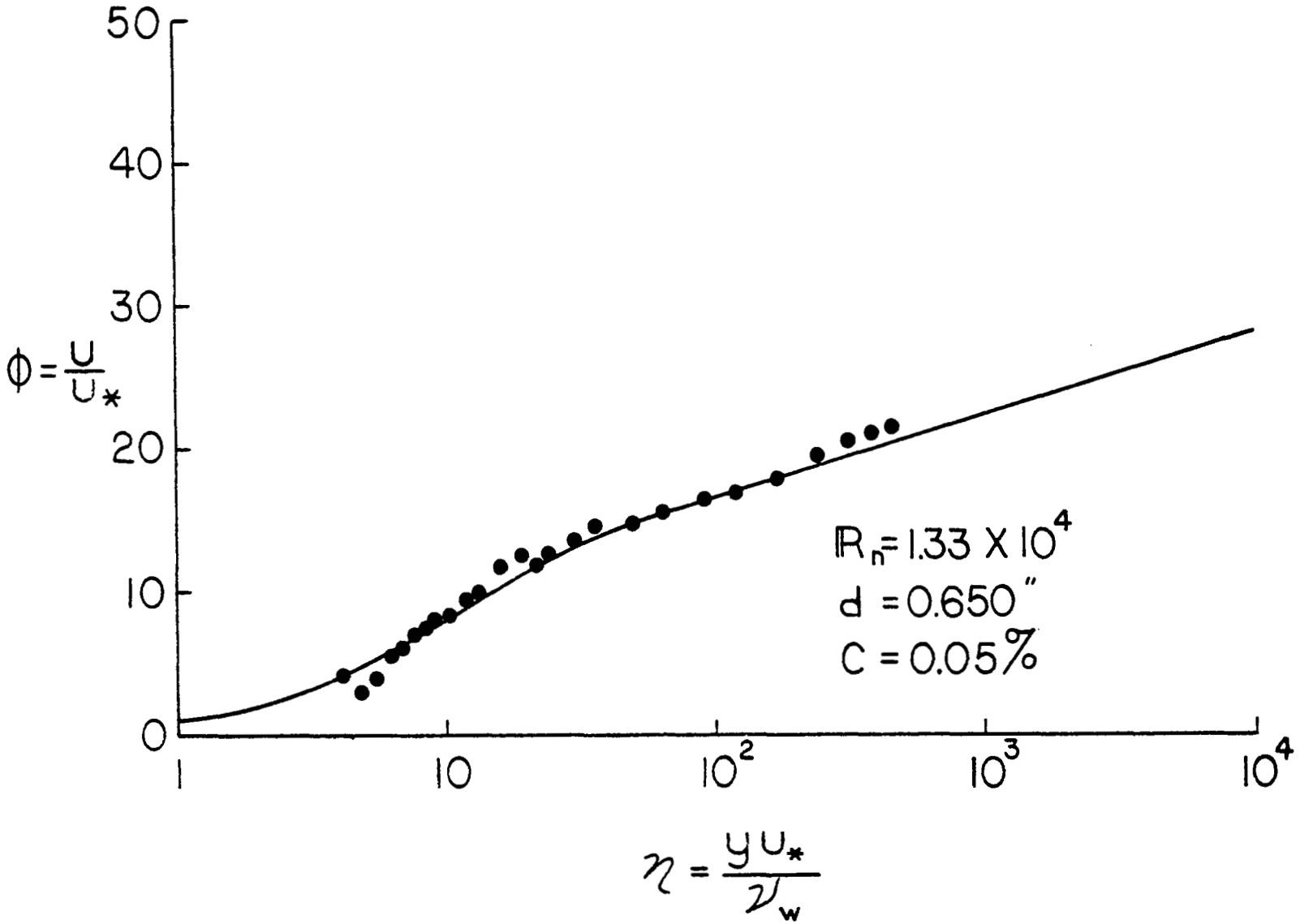

Fig. 7 Generalized Velocity Profile

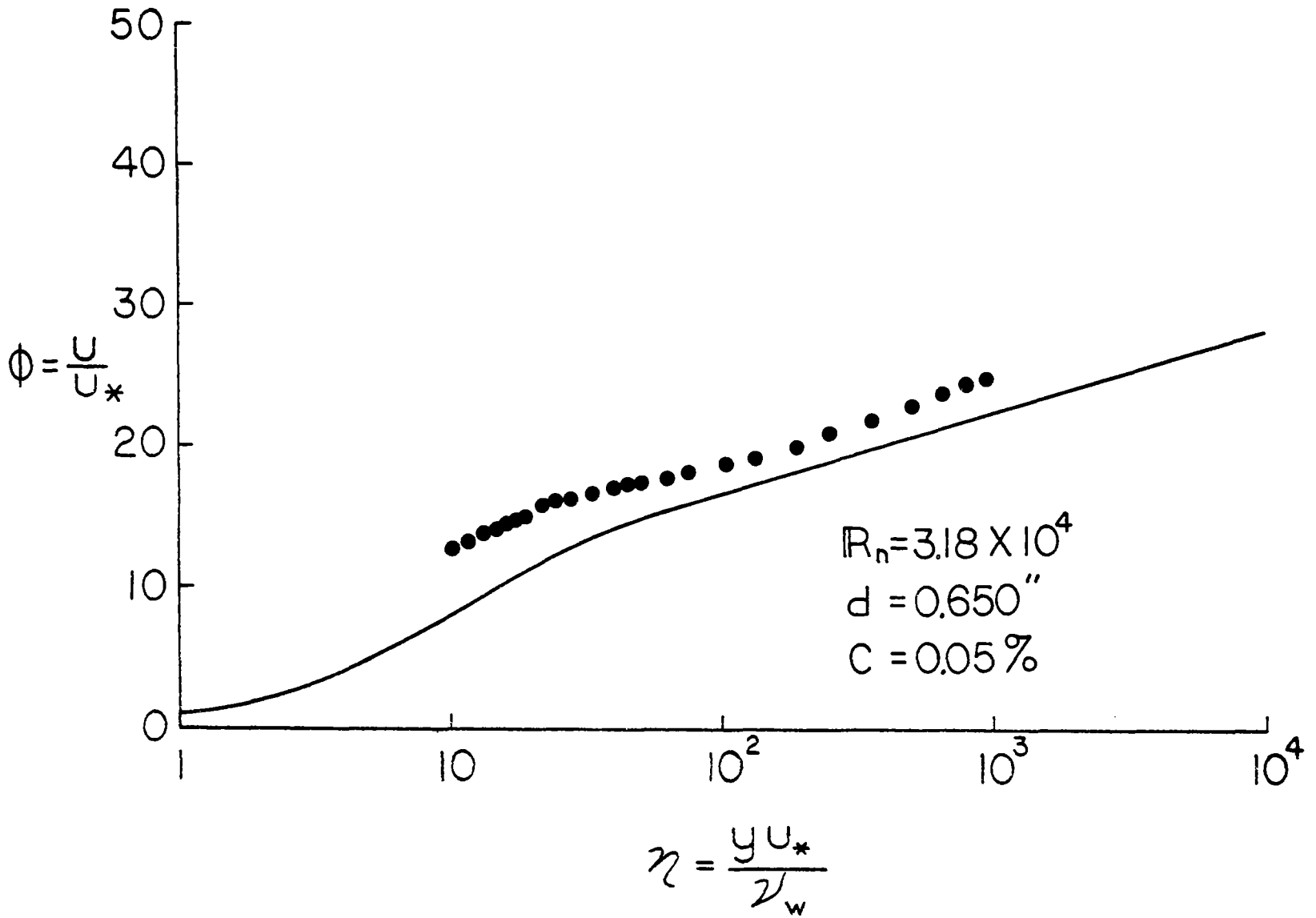

Fig. 8 Generalized Velocity Profile

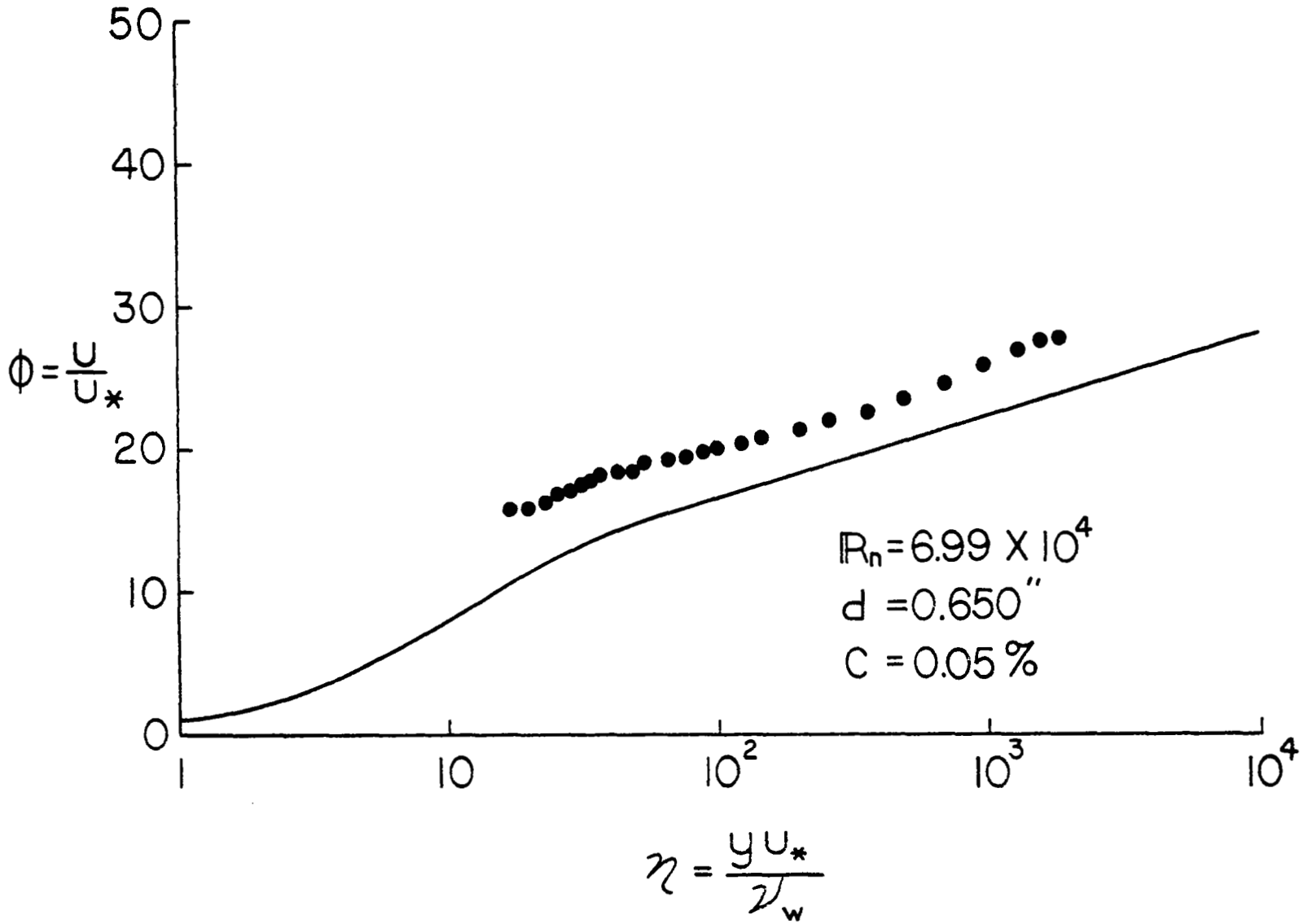

Fig. 9 Generalized Velocity Profile

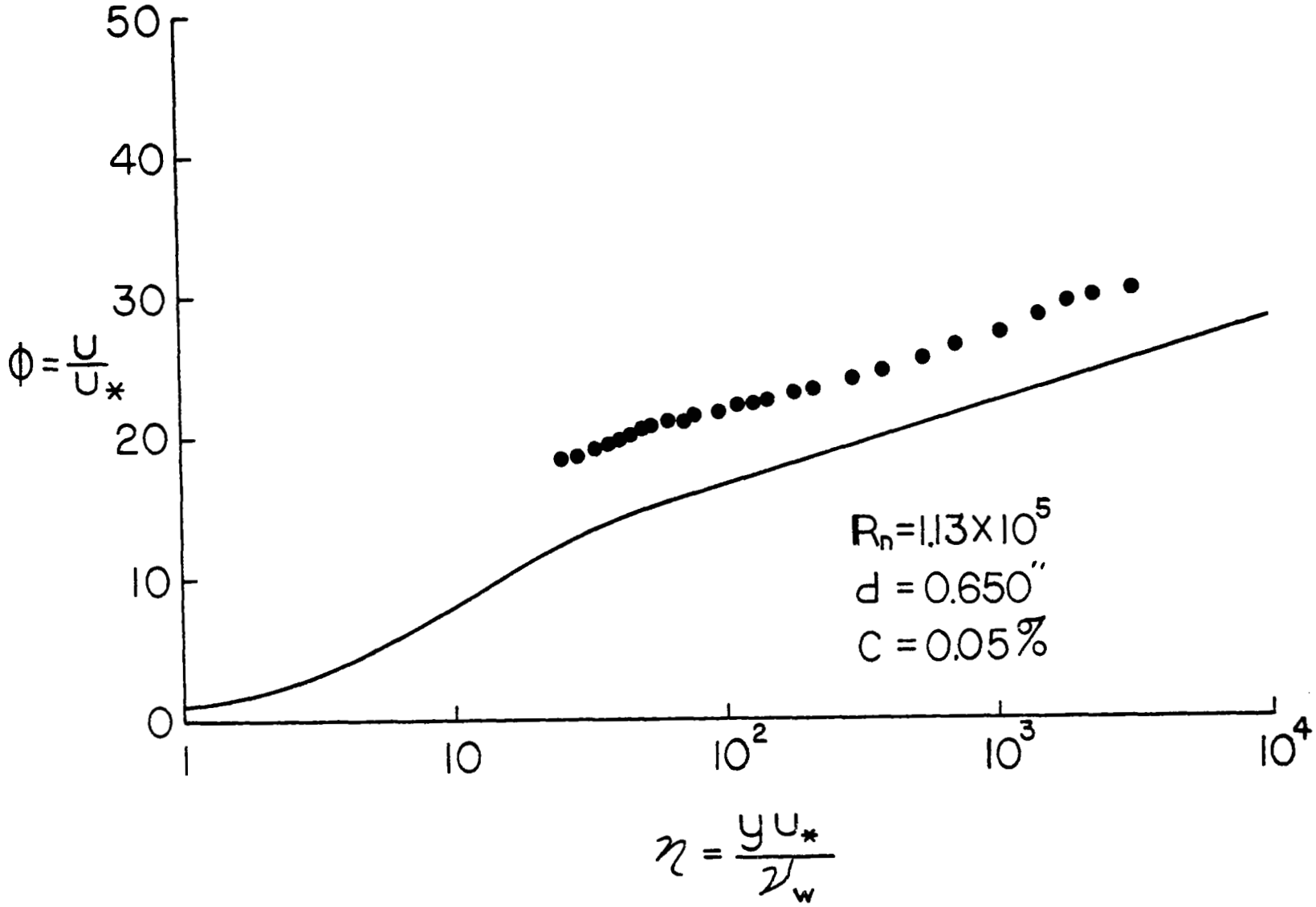

Fig. 10 Generalized Velocity Profile

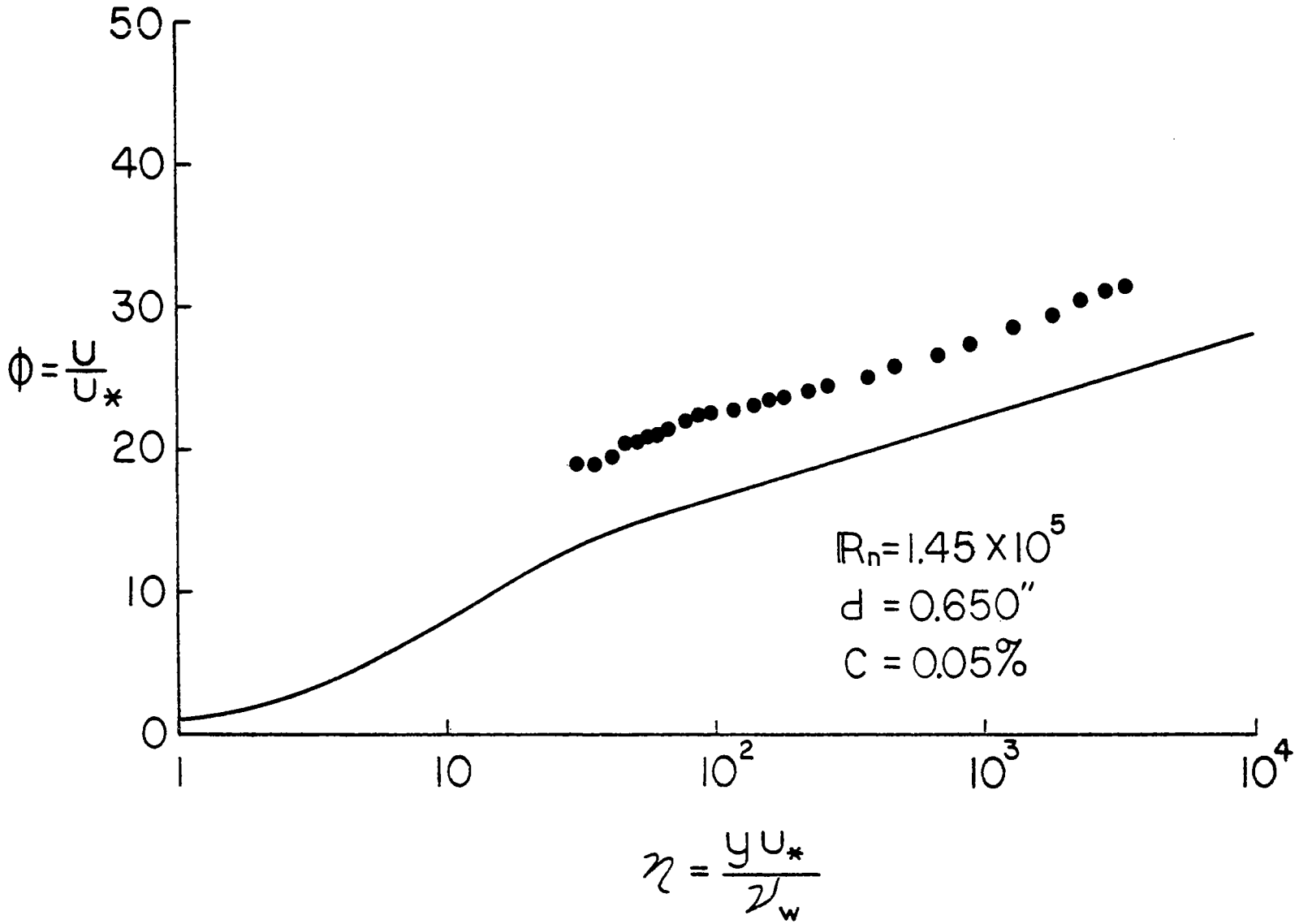

Fig. 11 Generalized Velocity Profile

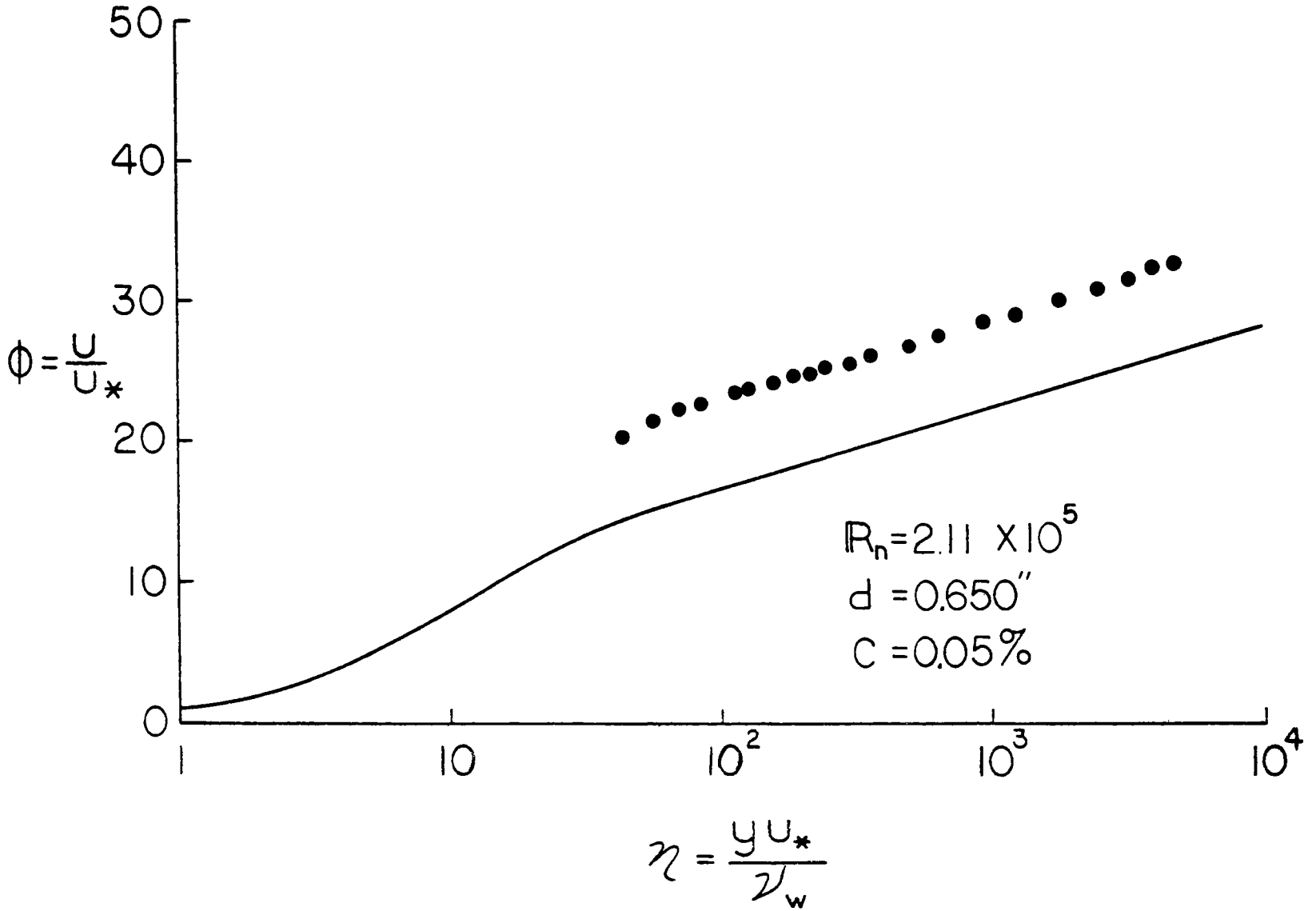

Fig. 12 Generalized Velocity Profile

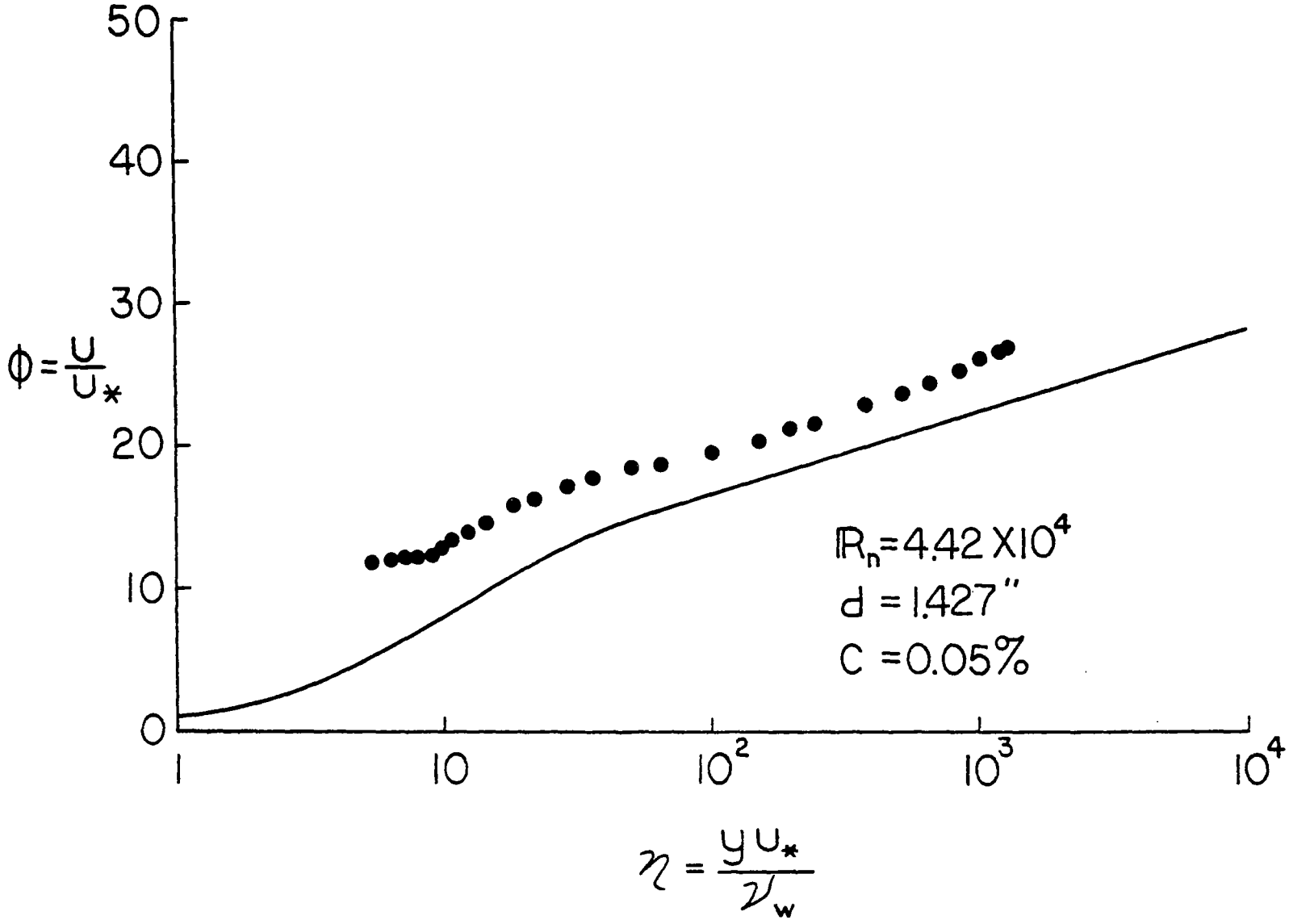

Fig. 13 Generalized Velocity Profile

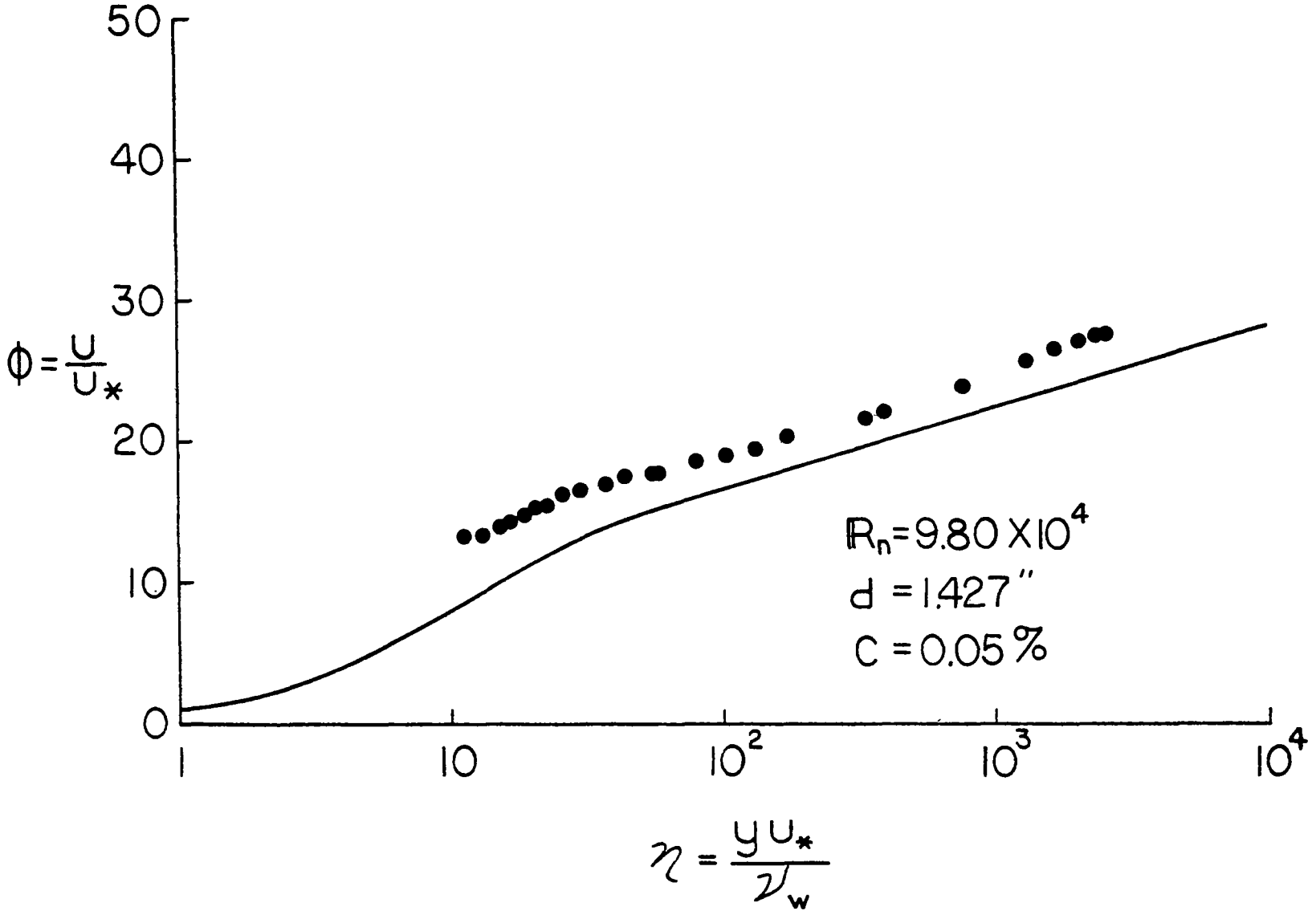

Fig. 14 Generalized Velocity Profile

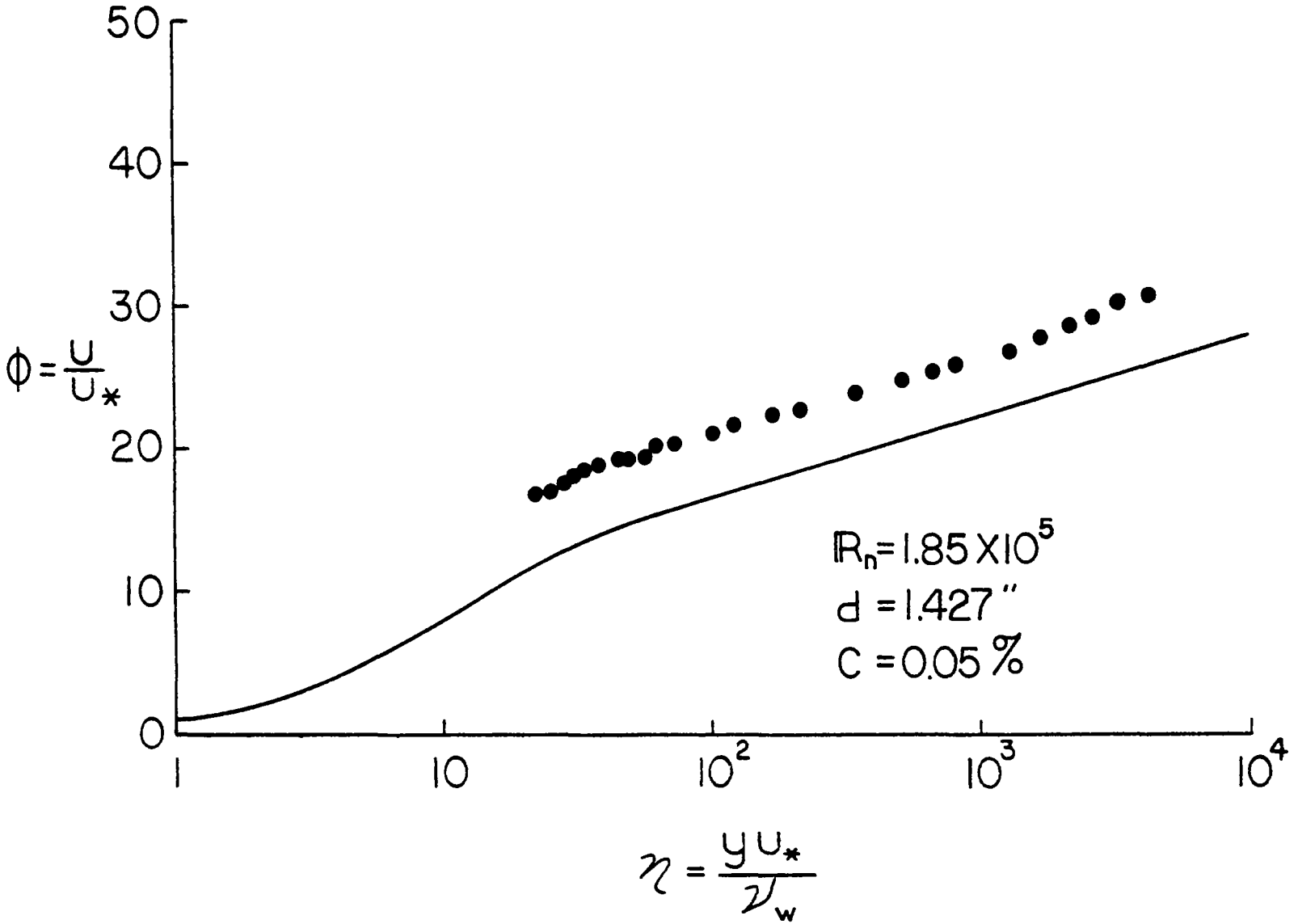

Fig. 15 Generalized Velocity Profile

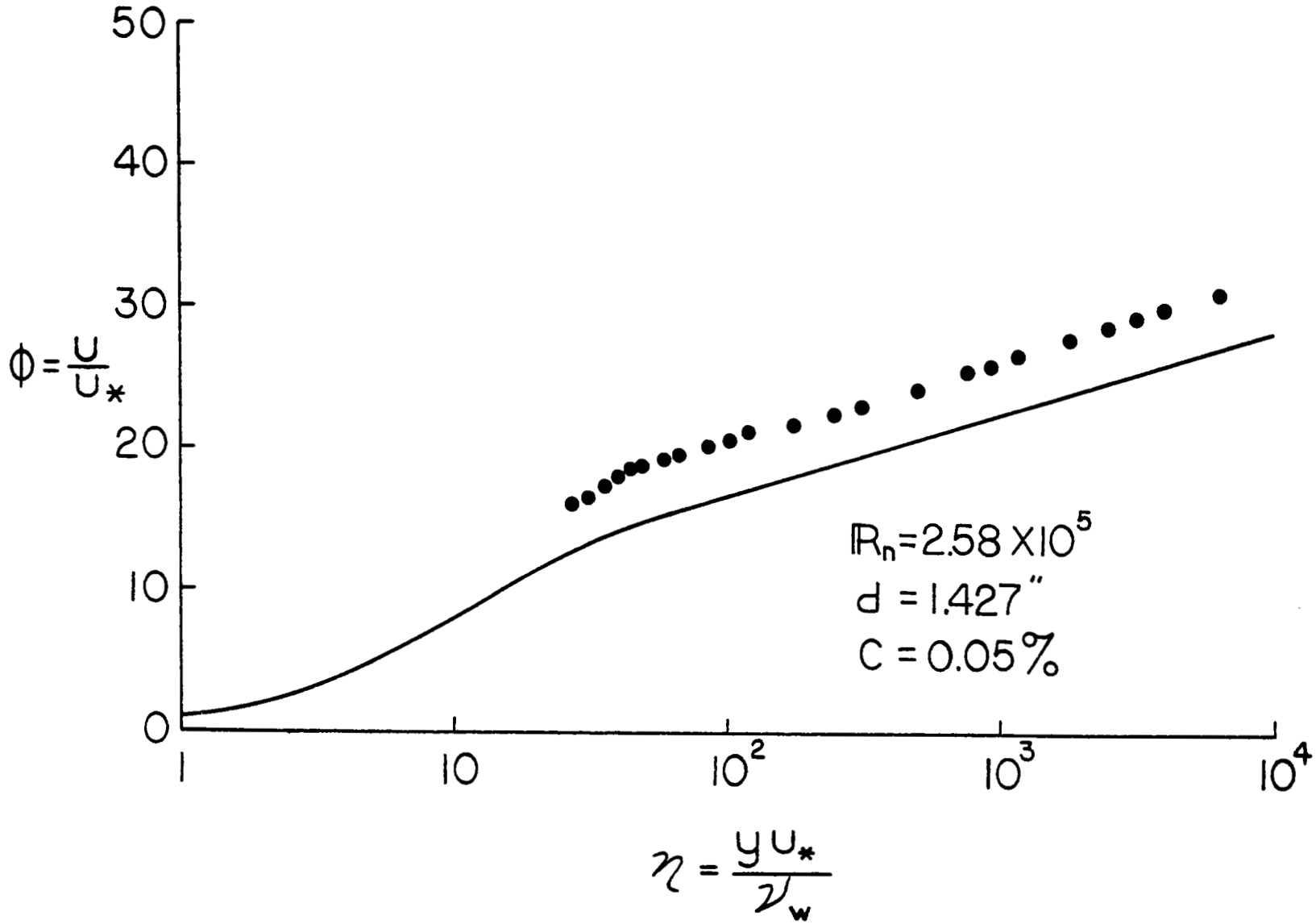

Fig. 16 Generalized Velocity Profile

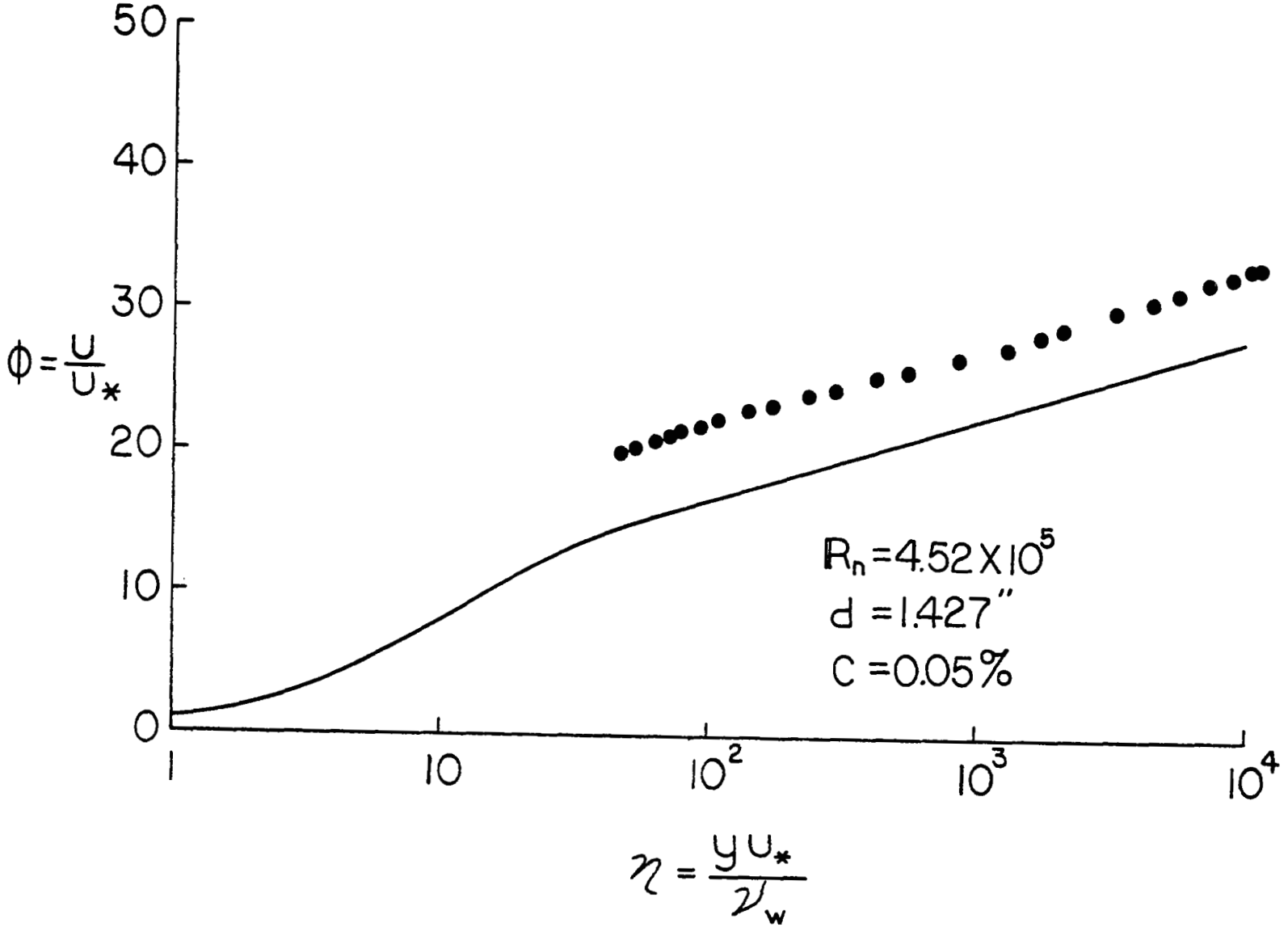

Fig. 17 Generalized Velocity Profile

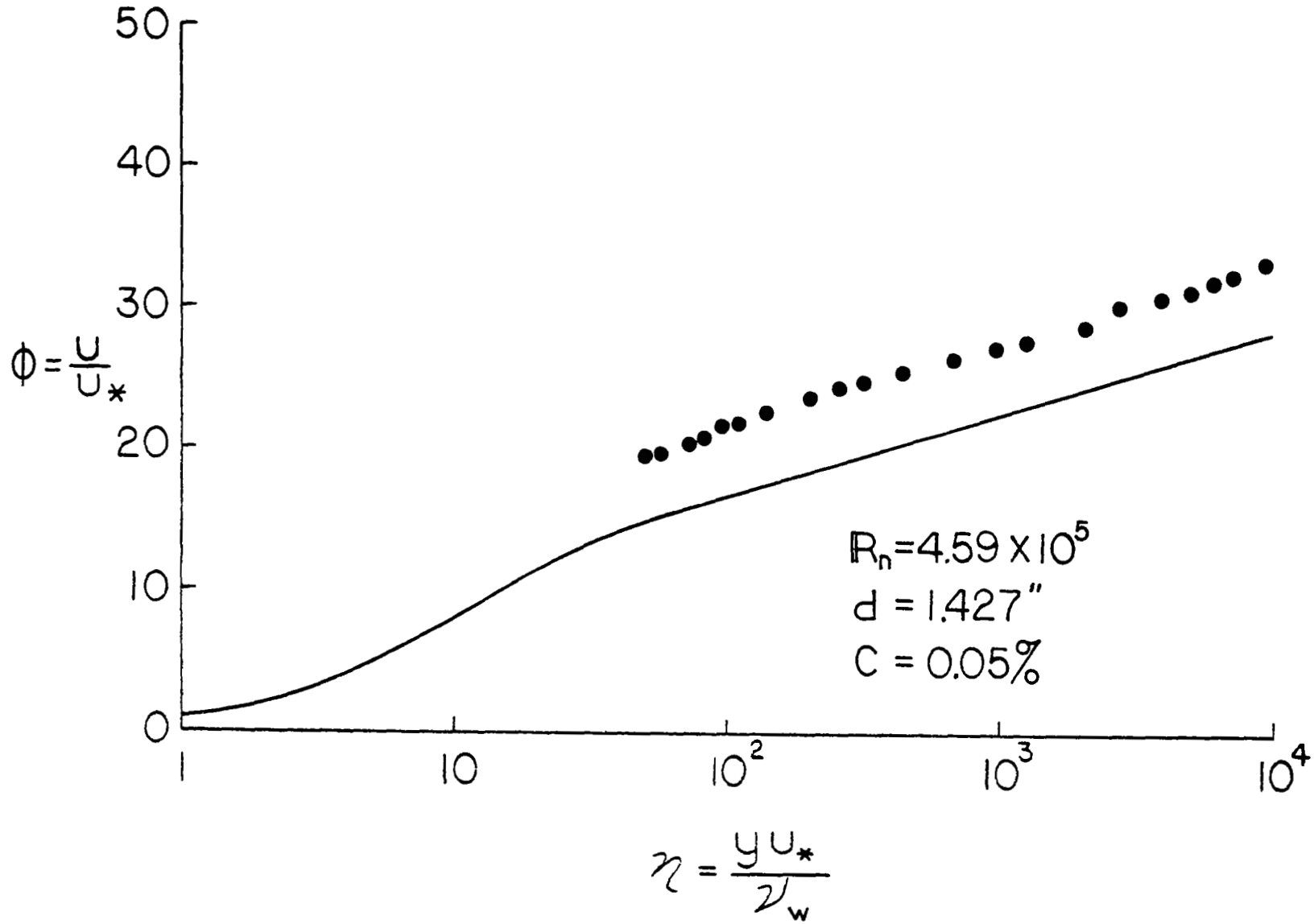

Fig. 18 Generalized Velocity Profile

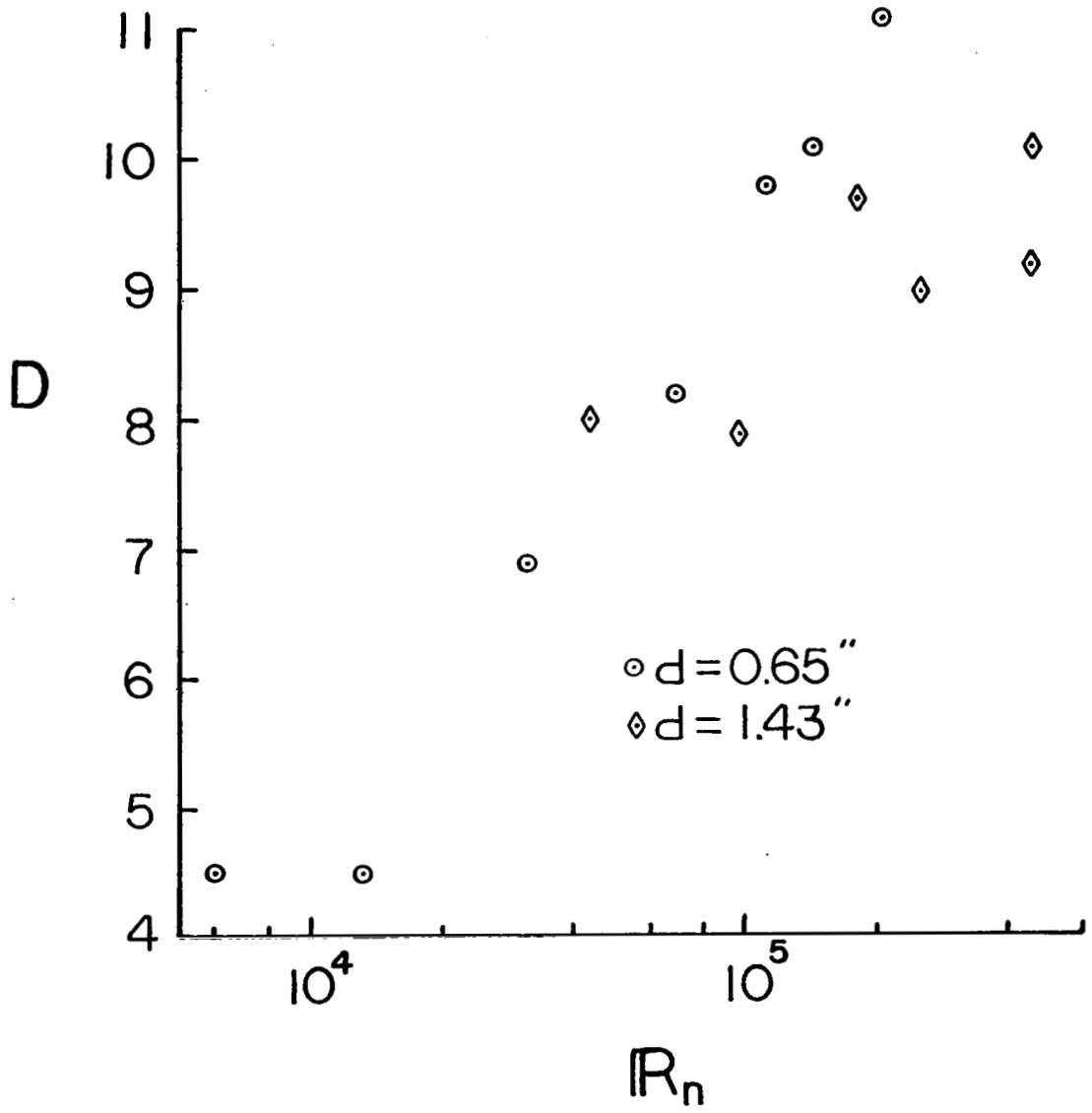

Fig. 19 Comparison of D for Small and Large Pipes as a Function of R_n

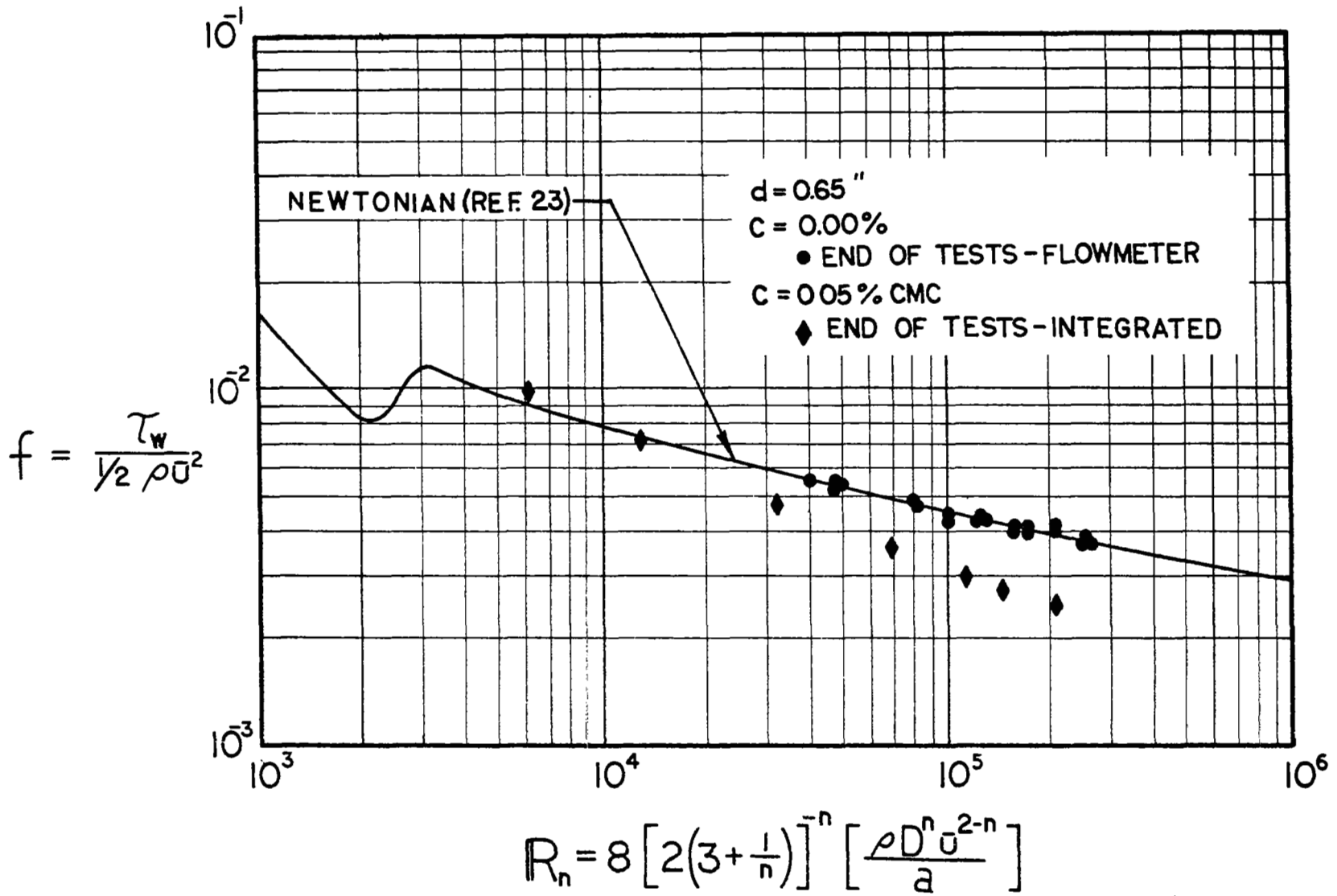

Fig. 20 Comparison of Friction Factors for 0.05% CMC and Water in the Small Pipe

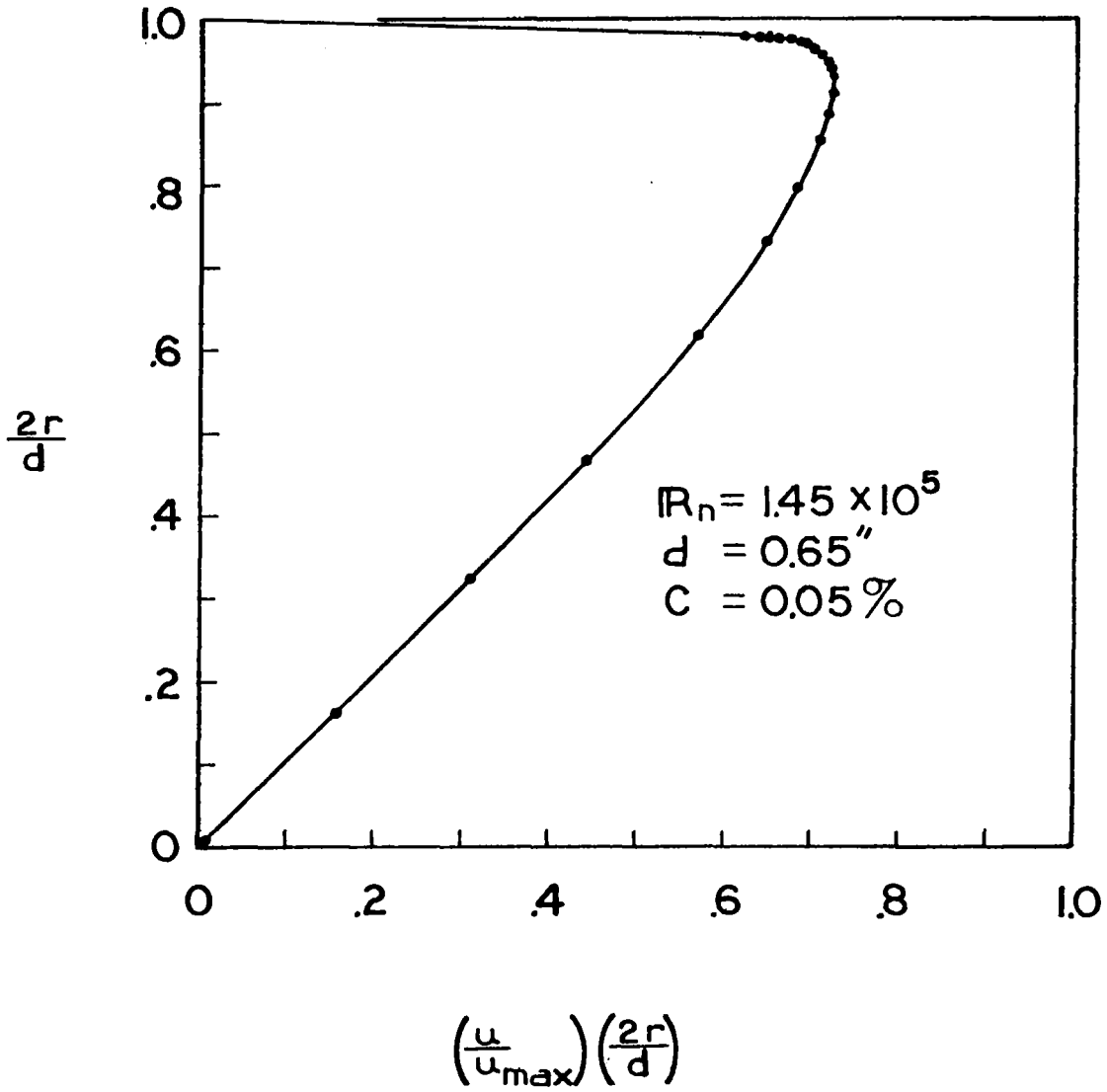

Fig. 21 Dimensionless Plot of Flow Rate Per Unit Area Versus Radial Position

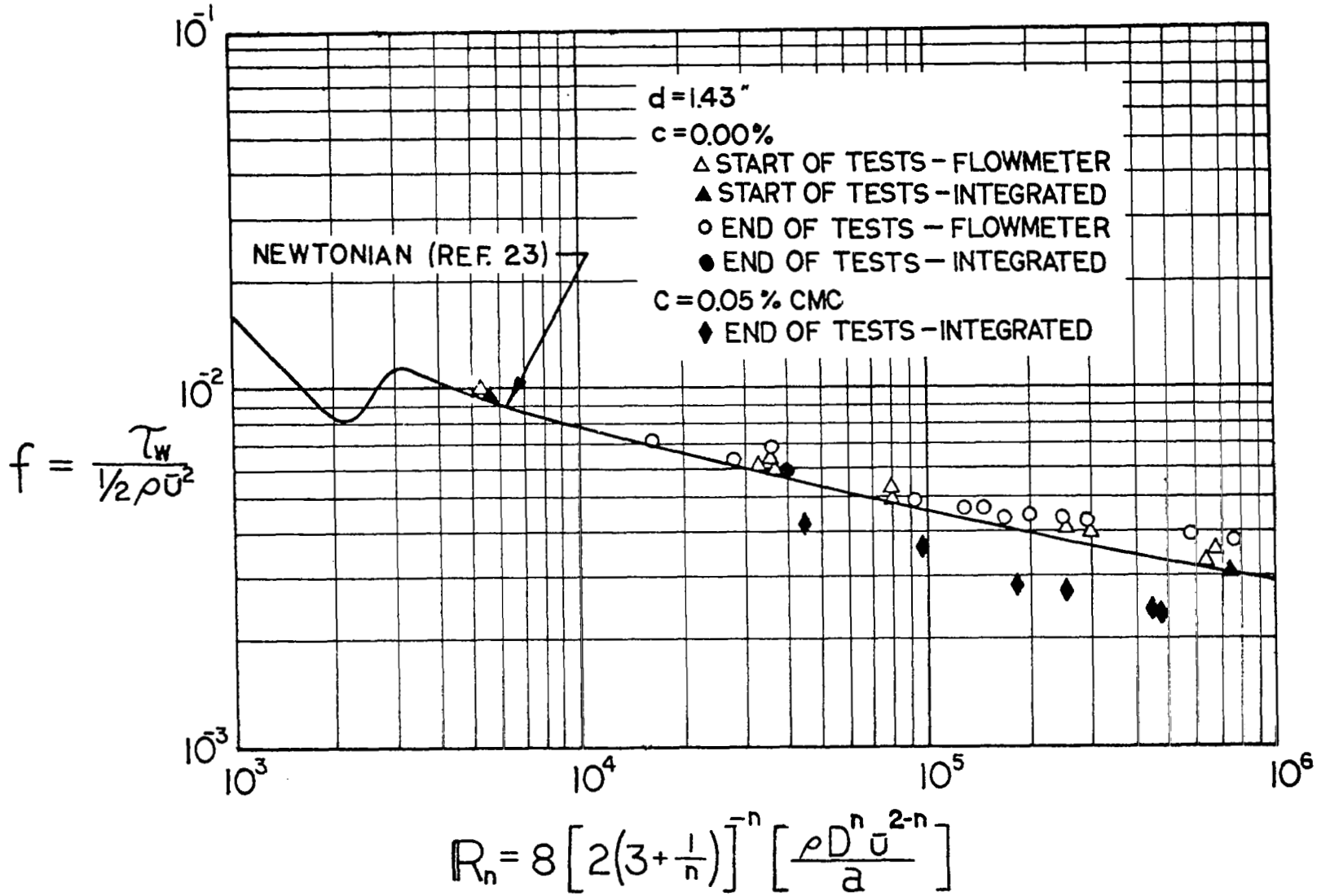

Fig. 22 Comparison of Friction Factors for 0.05% CMC and Water in the Large Pipe

NASA-Langley, 1966 CR-395